POLITECNICO DI MILANO

Department of Industrial and Information Engineering

Course of study in Biomedical Engineering

OPTIMIZATION AND CHARACTERIZATION OF A COMMERCIAL 3D PRINTER FOR DIRECT HYDROGEL WRITING

Supervised by:

Professor Marco Carminati

Co-supervised by:

Professor Jenny Emneus

Senior Researcher Arto Heiskanen

Master Thesis of:

Marianna Volino Matr.833257

Academic Year 2015/2016

Contents

List of Figures

List of Tables

List of Acronyms

A

AM *Additive Manufacturing*

C

CAD *Computer-Aided Design*

CT *Computed Tomography*

D

DAPI *4',6-diamidin-2-fenilindolo*

DIW *Direct Ink Writing*

DLP *Digital Light Processing*

DMD *Digital Mirror Device*

DTU *Technical University of Denmark*

E

ECM *ExtraCellular Matrix*

EEPROM *Electrically Erasable Programmable Read-Only Memory*

F

FDM *Fused Deposition Modelling*

G

GelMA *gelatin methacryloyl*

H

HCEC *Human Corneal Epithelial Cell*

HFIP *1,1,1,3,3,3-hexafluoro-2-propanol*

L

LCD *Liquid Crystal Display*

LED *Light Emitting Diodes*

M

MRI *Magnetic Resonance Imaging*

P

PEG *poly(ethylene glycol)*

PLA *polylactic acid*

PTMC *poly-(trimethylene carbonate)*

R

RP *Rapid Prototyping*

S

SD *Secure Digital*

SF *Silk Fibroin*

SF-G *Silk Fibroin-Gelatin*

SFF *Solid Free-Form Fabrication*

SLA *Stereolithography Apparatus*

SLC *Standard Language Compiler*

SML *Standard MetaLanguage*

STL *Standard Triangulation Language*

T

3D *Three-Dimensional*

3DP *Three-Dimensional Printing*

U

UV *Ultra Violet*

Abstract

Compared to other techniques to create scaffolds, three- dimensional (3D) bioprinting has exciting prospects for realizing 3D tissue constructs by delivering living cells with appropriate biomaterials. A technique for controlled deposition of hydrogels and cells in specific and complex architectures is described. It employs a three-dimensional positioning system with a piston-driven syringe to deposit hydrogel structures with a highly control on the flow rate. The system was characterized in terms of deposition parameters such as piston speed, hydrogel viscosity, line width and height. A high viscosity of the hydrogel it is necessary for filament shape retention during and after extrusion. A new ink for bioprinting applications was chosen: the silk fibroin solution derived from the Bombyx mori silkworm. Here representative examples of 3D silk fibroin structures assembled layer-by-layer (8-28 layers) are reported. The thesis project focused on the ink design and its deposition mechanisms. The fluid dynamics involved in the material extrusion and spreading play an important role in the characterization and the optimization of the system. The width and height of the printed lines are, indeed, influenced by the deformation of the material upon solidification. The solidification of the printed structures occurred thanks to solute evaporation at a temperature of the stage of 40 °C. The rheological behaviour of the silk fibroin solution was studied. The 25 w/v% silk fibroin solution exhibits a shear thinning behaviour: the lower viscosity was 1.64 Pa s. The line width does not vary depending on the flow rate at a given deposition speed but by varying the deposition speed it slightly decreases. Fixing the flow rate, with a certain line width, the height also results inversely proportional to the deposition speed. The lateral and vertical resolution of the deposition system are therefore determined by the ink rheology, the printing speed and the nozzle's diameter and shape.

Estratto

Il concetto di stampa in tre dimensioni (3D printing) fu introdotto per la prima volta nel 1983 da Charles W. Hull. È un processo di prototipazione rapida che consente la realizzazione di strutture tridimensionali, strato su strato, a partire da un modello digitale dell'oggetto. Le tecnologie di "3D printing" più comunemente utilizzate sono: la Stereolitografia (SLA), la tecnologia di Digital Light Processing (DLP), la Modellizzazione a Deposizione Fusa (FDM) e quella più recente di Direct Ink Writing (DIW). Nel corso degli anni, le tecnologie di stampa in tre dimensioni hanno acquistato una maggiore influenza nei campi più disparati: arte, architetture ed ingegneria dei tessuti.

Lo scopo dell'ingegneria dei tessuti è la rigenerazione, il ripristino o la sostituzione di tessuti o organi viventi che hanno subito lesioni o ingiurie durante il corso della vita. Per raggiungere questo scopo, strutture di supporto, comunemente chiamate scaffold, vengono utilizzate in applicazioni biomediche e di ingegneria dei tessuti con l'obiettivo principale di rigenerare o sostituire funzionalmente e strutturalmente i tessuti originari. In generale gli scaffolds devono possedere alcune caratteristiche preminenti: percorsi interni che consentano la migrazione e l'adesione cellulare, adeguate proprietà meccaniche, mantenimento della forma durante la crescita cellulare ed elevata porosità per consentire la proliferazione e la differenziazione delle cellule ma anche il trasporto di ossigeno, nutrienti, fattori di crescita e l'espulsione dei prodotti di scarto.

In questo ambito, le tecnologie di stampaggio in 3D consentono, rispetto a tutte le altre tecniche utilizzate per realizzare scaffolds, di ottenere una elevata ripetibilità e controllo sull'interconnessione dei pori, sulla loro distribuzione, taglia e volume portando alla realizzazione di strutture di supporto su misura. Due tipologie di scaffolds possono essere fabbricate con le tecnologie di 3D printing sopracitate: scaffold a-cellulari, in cui le cellule vengono seminate su una struttura appropriata

stampata in 3D e scaffolds bio-stampati, in cui le cellule e il biomateriale scelto vengono stampati insieme per formare la struttura tridimensionale.

La tecnologia di 3D bioprinting viene utilizzata per ottenere una distribuzione controllata delle cellule nelle strutture tridimensionali in modo tale che le cellule stesse non muoiano o perdano la loro funzionalità.

Lo scopo del progetto è stato quindi quello di esplorare una nuova applicazione della tecnologia di stampa in 3D nel contesto dell'ingegneria dei tessuti. Il progetto ha riguardato infatti l'ottimizzazione di una stampate 3D commerciale a basso costo per la deposizione controllata di idrogeli al fine di realizzare accurate culture cellulari tridimensionali. L'iniziale dimostrazione della fattibilità dell'adattamento della stampante commerciale per la deposizione controllata di idrogeli in geometrie tridimensionali potrebbe portare alla validazione di questa tecnica per la realizzazione di tessuti e modelli cellulari.

Grande importanza ha assunto inoltre la scelta e la progettazione del materiale da stampare. Il progetto di tesi ha infatti dimostrato come siano la scelta del materiale e le sue caratteristiche ad influenzare l'ottimizzazione del sistema di deposizione e non viceversa.

Il sistema di deposizione è costituito da una stampante 3D, Felix 3.0 Dual extruder, e da un sistema semplice, chiamato "estrusore di pasta", il Discov3ry, che viene elettricamente connesso alla stampante e consente l'estrusione del materiale esercitando una pressione controllata sul pistone di una siringa. Questa modalità di estrusione è tipica delle tecniche di DIW filament- based dove un materiale altamente viscoso viene estruso sotto forma di filamento continuo su un supporto mobile, in questo caso il piatto della stampante, attraverso un ugello cilindrico o di forma conica.

Le prove sperimentali hanno evidenziato due problemi principali: il non perfetto controllo della quantità di materiale estruso per unità di tempo (portata) e l'inadeguatezza meccanica del supporto realizzato dall'azienda per consentire l'eventuale utilizzo della punta del Discov3ry come un secondo estrusore della stampante.

Riguardo quest'ultimo problema, l'obiettivo è stato quindi quello di costruire un supporto che consentisse di calibrare facilmente la punta dell'estrusore di pasta senza comprometterne la capacità di movimento lungo l'asse Z. Il supporto finale realizzato si è inspirato al design dell' hot-end della stampante.

È importante sottolineare però come il fluido non venga riscaldato in alcuna parte del sistema di estrusione, che consente solo estrusioni a temperatura ambiente.

È stato possibile invece controllare la portata attraverso la comprensione delle leggi meccaniche e fisiche che regolano il fluire del materiale lungo il sistema.

Il Discov3ry si comporta come una pompa a siringa costituito da: un motore passo-passo, una trasmissione, due ruote dentate e una vite senza fine vincolata alla base in cui viene alloggiata la siringa. Potendo controllare le rivoluzioni del motore passo-passo grazie al software della stampante e noto il rapporto di riduzione dell'intero sistema, è stato possibile determinare la velocità di traslazione della vite e dunque la portata in uscita dalla siringa.

La scelta del materiale è ricaduta su un nuovo tipo di idrogelo naturale, impiegato da pochi anni in ingegneria dei tessuti: la soluzione di fibroina di seta.

La soluzione di fibroina di seta è un idrogelo naturale, estratto a partire dai bachi da seta Bombyx mori, che ha mostrato di essere altamente biocompatibile e possedere ottime proprietà meccaniche. In seguito al processo di estrazione, la soluzione ottenuta è una soluzione di fibroina di seta al 7-8 w/v%. Tale soluzione dal punto di vista reologico risulta essere simile all'acqua; essa quindi è stata estremamente utile in fase di comprensione e modellizzazione del sistema ma non successivamente per la realizzazione di strutture multi-strato. Materiali altamente concentrati hanno mostrato di essere particolarmente adatti per realizzazione di specifiche strutture tridimensionali in quanto capaci di mantenere la forma filamentosa anche a seguito dell'estrusione. Di conseguenza è stato necessario concentrate la soluzione per ottenere una risposta di assottigliamento al taglio ("shear thinning response"). Questo significa che aumentando la pressione o la velocità di estrusione al di sopra di un certa soglia ("shear yield stress"), la soluzione inizierà a fluire con una sempre minore viscosità e quindi risulterà più facile da stampare ma, non appena estrusa, tornando ad una condizione di sforzo nullo, essa si comporterà come un gel.

E’ stato possibile concentrare la soluzione di fibroina di seta solo fino al 25 w/t%; essa ha mostrato una iniziale risposta di assottigliamento al taglio ma una viscosità non sufficiente per formare un filamento continuo che mantenesse la forma subito dopo l’estrusione.

La soluzione è stata, quindi, estrusa sotto forma di gocce. La fluidodinamica coinvolta nella formazione delle gocce e nella loro dilatazione a seguito dell’impatto con il substrato o con gli altri strati sottostanti gioca un ruolo fondamentale nella determinazione della risoluzione laterale e verticale del sistema. L’altezza e la larghezza delle linee stampante dipendono dalla taglia, dall’estensione della dilatazione e dalla deformazione delle gocce inseguito a solidificazione.

La solidificazione delle strutture avviene in seguito all’evaporazione del contenuto d’acqua della soluzione di fibroina di seta grazie ad una temperatura del piatto della stampante di 40°C.

La migliore risoluzione laterale ottenuta con il sistema utilizzato (ugello di forma cilindrica piatto con diametro interno di 610 μm ed esterno di 900 μm) è stata 850 μm ad una velocità di deposizione di 15 $\frac{mm}{s}$. La larghezza di linea non varia in dipendenza della portata ad una data velocità di deposizione ma variando la velocità di deposizione diminuisce leggermente. Fissando la portata, con una certa larghezza di linea, anche l’altezza risulta inversamente proporzionale alla velocità di deposizione. Uno spessore di 40 μm è stato ottenuto con lo stesso ugello, ad una portata di 0.4 $\frac{mm^3}{s}$ e una velocità di deposizione di 2 $\frac{mm}{s}$.

Sono state realizzate anche strutture a più strati. Il profilo di queste strutture è risultato non perfettamente uniforme; questo potrebbe essere dovuto al profilo rotondo delle singole linee stampate che non favorisce un supporto adeguato o alla non perfetta fusione del materiale depositato strato su strato.

La risoluzione laterale e verticale del sistema di deposizione sono quindi determinate dalla proprietà reologiche della soluzione, dalla velocità di stampa, dal diametro e dalla forma dell’ugello.

Il sistema è stato quindi caratterizzato in termini di parametri di deposizione quali la viscosità del materiale, la larghezza e l’altezza di linea. Sono state riscontrate

numerose limitazioni dovute alla scelta del materiale usato e alla natura del sistema. In ogni caso esso ha mostrato buone potenzialità per essere adottato nel campo del 3D bioprinting; inoltre è facile da usare e non troppo costoso.

CHAPTER 1
INTRODUCTION

The three- dimensional (3D) printing technology emerged over 30 years ago, though it really burst into the scene in the last 5 years, bringing to major innovations in many areas, such as engineering, manufacturing, art, education and medicine.

The real driver for this technique is that it enables the creation of highly complex structures in just few hours. The time that elapses between an idea and a functioning prototype is significantly lower than that which can be achieved with any other kind of technique used so far.

In the last few years, the technology has brought affordable, easy-to-use, consumer-grade models of 3D printer to market with different costs and characteristics. The cost of a 3D printer spans from around one thousands to one million of dollars and depends on many factors such as the type of the 3D printer, the material used, the size of the printed object, how many units you can print and the end-use of the 3D printed structure. Thanks to the lowering of costs, it is now possible to print almost everything also at home; from smartphone cases to every-day object creating as many items as you desire with minimal effort and making things rather than buying them.

Recent advances have enabled 3D printing of biocompatible materials, cells and supporting components into complex 3D functional living tissues nevertheless this involves additional complexity: the choice of materials, cell types, growth and

differentiation factors, and technical challenges related to the sensitivities of living cells and the construction of tissues.

As a matter of fact, the use of 3D printing technology in biomedicine has been mostly limited to the fabrication of prosthesis (in a purely mechanical perspective).

The aim of this project was therefore to explore a novel scientific application of 3D printing technology (spanning from industrial manufacturing and professional fast prototyping, down to personal fabrication) in the context of micro-scale cellular manipulation and study.

The project involved the optimization of a low-cost commercial 3D printer for controlled deposition of hydrogels for the accurate realization of three-dimensional cells culture.

The first demonstration of the feasibility of adaptation of a commercial printer for spotting cells in 3D geometries in a controlled way and with sub-mm resolution could bring to the validation of this technique to realize tissues and models organs.

The latter expected result is a high-risk task, with correspondingly, a relevant impact in biomedicine and bio-micro-technology.

Aim and Objectives of the Project

The thesis focused on various aspects of the 3D printing technology, starting from the understanding of the basic principles that characterize the traditional 3D printing techniques to the application of these principles to a new optimized system for liquid deposition and the realization of a final hydrogel-based structure.

In tissue engineering, 3D printing allows the combination of cells and materials together in a way that recreates a specific architecture. The structure of the tissue is very important in its function. When you look inside the body the tissues have very particular architectures which are basically different cells types coming together and organizing in a very specific manner.

Some of the major obstacles in 3D printing technology applied to biological issues are associated with the ability to create different kinds of structures and with the choice of the material that you are going to print.

In respect to the former there is the need to choose the correct technique that allows the cells to remain viable and to get the proper resolution, allowing the cells to self-assemble and get the right kind of architecture and function. There are, therefore, a lot of scientific challenges related to what exactly you are going to print, what kind of material, what kind of cells, how you can control the biological and biophysical signals that direct the cells, and technical challenges related on the manufacturing process, its feasibility, its reproducibility, its accuracy.

The main difference between “3D printing” and “3D bioprinting” is often the kind of ink that you use. The choice of a biological inks has a strong impact on the type of manufacturing and the type of conditions in which you are going to print.

Thus, the main goal of the project was the optimization of a “nozzle”.

The term “nozzle”, in this context, is not barely a component of a 3D printer but includes, on one hand, the deep investigation of the right properties of the material that make it printable and biocompatible and, on the other hand, all the different solutions that have been found to solve the technical issues (such as the achievement of a correct and stable calibration of the deposition system).

It represented the first step in a research path that wants to bring to the achievement and the excess of the results already seen in tissue engineering by using a very low-cost 3D printing system.

The work comprised the following objectives:

1. Study of the current state of the art concerning 3D-printing, hydrogels and three-dimensional scaffolds;
2. Setting up of the printer and adaptation to handling hydrogels;
3. Optimization of the printer and of the material (viscosity of the hydrogel) for correct extrusion with the desired spot size;
4. Assessment of the limits (resolution, i.e. minimum spot/droplet size that can be deposited, lines width and thickness, speed, thermal issues) of this technique with respect to the goal of realizing complex 3D cell colonies.

Short Description of the Thesis Content

The Master thesis covers all the work done in 7 months at the department of DTU (Technical University of Denmark) Nanotech in collaboration with the Bioanalytics group of Jenny Emnéus. The purpose of the project was to set the bases for future studies and developments. It comprises six chapters:

- Chapter 2 "3D Printing Approaches in Tissue Engineering" introduces the state of the art of 3D printing approaches, describing their basic concepts and highlighting their main advantages and drawbacks with a particular interest on their recent applications in tissue engineering. Three typical kinds of techniques used in biomedical field are presented: stereolithography, digital light processing and fused deposition modelling. Due to the significance of the direct ink writing technology as a part of the experimental work, its characteristics were also summarized.

- Chapter 3 "Deposition System" describes the experimental set-up. It presents the characteristics of the deposition system (all the laws that govern the ink printing process) and all the optimizations that have been implemented to achieve a correct and stable calibration of the system.

- Chapter 4 "Ink Design" describes the properties and the design of the chosen ink explaining the reason of the selection of this material compared to other ones.

- Chapter 5 "Results and Discussion" presents an overview of all the achieved results comparing them with those seen in literature so far.

- Chapter 6 "Conclusions and Future Perspectives" summarizes the key conclusions of the work and shortly describes future perspectives.

CHAPTER 2
3D PRINTING APPROACHES IN TISSUE ENGINEERING

Tissue engineering also called “regenerative medicine” refers to attempt to create functional human tissue from cells in a laboratory. Its ultimate goal is to be a cure not merely a treatment by repairing and replacing tissues or organs that fail due to diseases, genetic errors, congenital abnormalities or traumatic injuries [1].

In the XXI century the life expectancy of the aged population increased and the elderly expects good quality life with high levels of activity. However, as we grow, our tissues fail; they fail due to illness or injury or simply the aging process and this can lead to a significant loss of quality life, particularly in individuals with chronic diseases.

Unfortunately it is possible to observe this degeneration since the age of 30-35 and around the 10% of the world’s population needs, at least, a tissue repair or replacement at some point during its lifetime. There are of course current options for tissue repair and replacement but all of these have limitations. None of these fully restore tissue function and the quality of life and the majority of them fails to grow and develop within the individual. Therefore it is imperative to ensure that any new regenerative medical technology solution for the aging population meets not only the clinical needs and increase patient expectation but also that is affordable in order to be clinically adopted.

In this perspective, 3D printing offers a promise to revolutionize patient's care.

The term "3D printing" refers to a process where a three-dimensional structure is fabricated layer by layer from the bottom up to the top surface. The successive layers of the object, that can have any shape or geometry, are formed under computer control thanks to a digital design of the structure [2].

The 3D printing technique is an additive manufacturing technology that had a big impact on a lot of markets, especially on the biomedical one. In medical practices being able to customize a product gives the possibility to create something that is patient specific. Nowadays, the 3D printing technology provides the 96% of the hearing aids worldwide and reproduces exactly the anatomy of that part of the body. It also enabled the reduction of surgery time giving the possibility to the surgeon to rehearse the procedure before the operation (i.e. what tool to use, where to cut and how to cut). Indeed, it is possible to create surgical templates or models that allows the surgeon to look an object or a part of the body in a 3D fashion, facilitating the surgical approach.

Several 3D printing techniques have been developed since the last 30 years and each of them has its own advantages and drawbacks. The main difference between these approaches lies in the choice of the material and how it is deposited.

Today we can print with metals, ceramics, polymers and biodegradable materials but after the emergence of the 3D bioprinting or "organ printing", as it is called, we can go a little bit further as well.

A human organ, like a building, is a collection of parts that has to come together and work together. A single block is not enough. Robert S. Langer and Joseph Vacanti realized that to build an organ a framework that guides the cell's growth is needed; a "scaffold" to define the parts and hold them together [3]. The challenge was, therefore, to engineer scaffold materials where living tissues can grow onto. But choosing the right material for a scaffold is only the first step in the process of creating a living body part.

In the conventional view of tissue engineering three elements would be necessary:

human cells (usually stem cells), biological signals such as pharmacological agents that can be used to restore cell function, and complex biomaterials porous scaffolds and matrices.

3D printing, or Solid Free-form Fabrication (SFF) technnology, in tissue engineering allows two different approaches: first of all, to build a-cellular 3D scaffolds (or molds) shaped into an organ-like structure and second to print scaffolds directly with living cells (bioprinted scaffold).

The first approach is the most common one and consist of two steps: make the scaffold and then put cells on top of it. In this way the cells can grow only on top of the scaffold and they cannot go inside it, slowing down the remodelling process. The second one, instead, is the most innovative one because allows to include cells into the scaffold with an extremely precise spatial distribution.

The advances in 3D bioprinting have enabled to form cellular models for 3D in vitro biology (Fig. 1). Wu et al. used a 3D hydrogel-based cell-laden technique to print human corneal epithelial cells (HCECs). Human corneal epithelial cells (HCECs), which are native resident cells of the cornea connected to form a dense plasma membrane, were applied for seeding onto some substrates, such as amniotic membranes, collagen gel and polycarbonate membrane, to generate a bioengineered corneal epithelium [4].

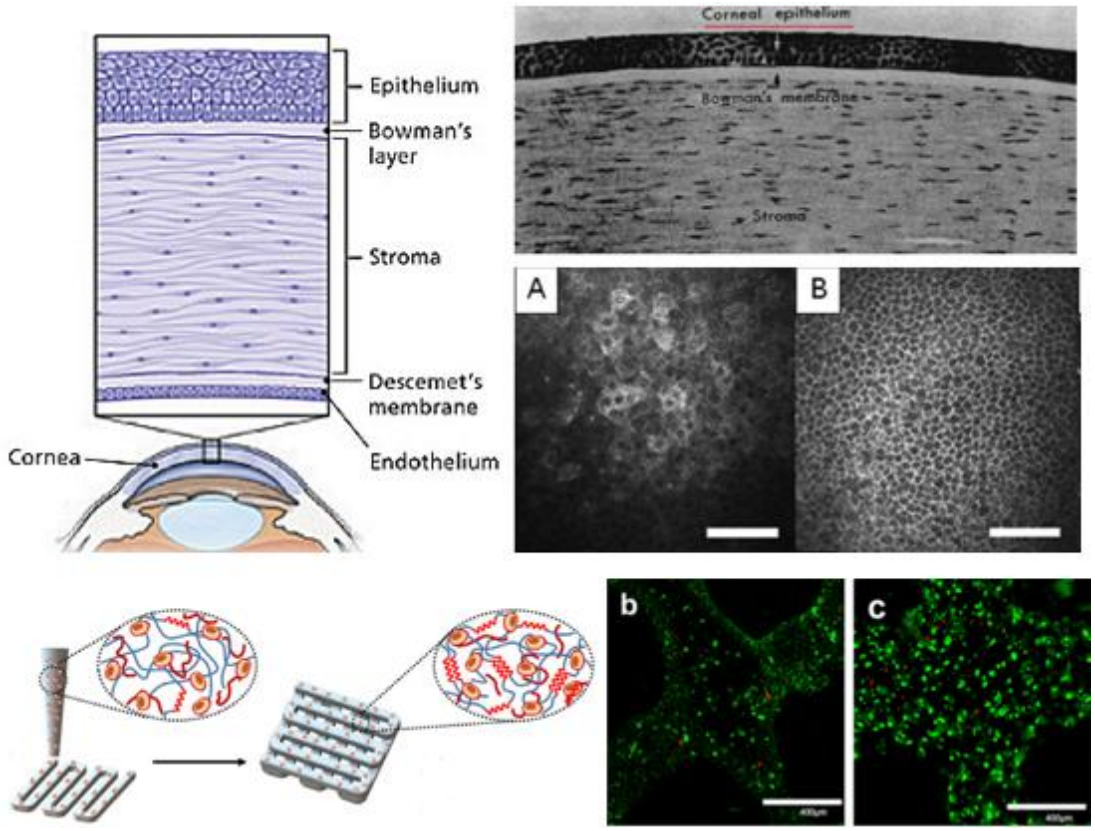

Figure 1 Top: on the left, schematic view of the anatomy of the cornea [5]; on the right, cross-section of a human cornea [6] (A. superficial epithelial cells, B. basal epithelial cells; scale bar, 100 μm [7]). Bottom: on the left, schematic elucidating the bioprinting of a 3D cell-laden construct with human corneal epithelial cells (HCECs)/collagen/gelatin/alginate hydrogel; on the right, human corneal epithelial cell viability after printing by live/dead staining (red: dead, green: live) (scale bar, 400 μm) [4].

Compared to other technologies to make scaffolds, 3D (bio)printing greatly reduces the human difference factor realizing custom-tailored scaffolds and allows the recast of the fabricated scaffold [8]. It is important to say that 3D printing complex structures like organs are still far away from us but the research on the basic techniques is flourishing.

In this chapter, four different approaches of 3D printing used in tissue engineering are presented: stereolithography, digital light processing, fused deposition modelling and the most recent direct ink writing techniques.

A final comparison table of all the four different 3D printing technologies can be found at the end of the chapter.

Stereolithography (SLA)

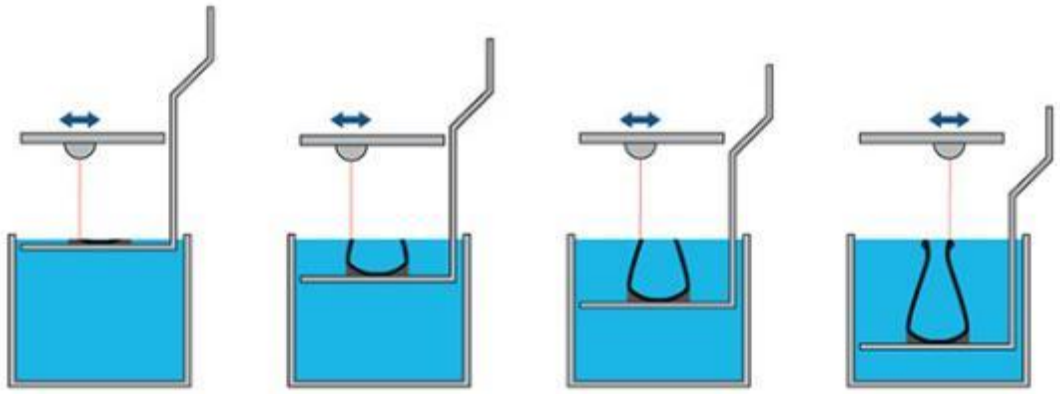

Figure 2 Section view of the printing process [9]

In 1983 Charles W. Hull developed stereolithography, the first commercial rapid prototyping technology that led to what is nowadays commonly known as 3D printing [10].

This process takes advantage of the distinguishing feature of a liquid plastic that hardens when it is exposed to UV light. A special laser outlines the design turning the material into solid, shaping the desired object. The laser can be focused using a set of lenses and then reflected with a motorized scanning mirror or, alternatively, it can be directly moved using an XY stepper motor arrangement (Fig. 2).

Once the first layer has hardened, the object is lowered and other resin is applied onto it, allowing the laser to harden the next level. One layer at the time, thousands of individual layers are adding, resulting in a three-dimensional object that emerges gradually layer by layer.

The hardening process goes by the name of Photocrosslinking.

Photocrosslinking means the photoinduced formation of a covalent bond between two different parts of one macromolecule. When exposed to light, the initiators, presented in the solution, produce free radicals that crosslink the monomers of the resin, starting the phase transition.

Stereolithography´s success in the automotive industry allowed 3D printing to achieve industry status and the technology continues to find innovative uses in many fields of study. The main advantages of this technology, beside the speed, are the perfect resolution (20 – 200 μm of layer's thickness) and the exquisite details achievable. In stereolithography, control of the thickness of the layer that is cured is essential [11]. For a given material, the cure depth is mostly determined by the energy of the light to which the material itself is exposed. This energy can be controlled by adjusting the power of the light source, and the scanning speed. Regarding accuracy and resolution, stereolithography is superior to all other SFF traditonal technologies.

In the biomedical field, stereolithographic models are used as an aid to diagnosis, preoperative planning and implant design and manufacture. Clinical images such as CT scans, X-ray and MRI images and any method that creates cross-sections of a physical object can be used to recreate a virtual model of the part of interest.

This allows to obtain patient-specific models and functional parts.

Madrazo et al. present two case studies in which stereolithography has been used to fabricate solid plastic replicas of spine from computed tomographic and magnetic resonance images [12]. Other tailored parts, such as hearing aids, are now routinely manufactured using stereolithography.

In many studies in literature, stereolithography has been utilized also to prepare molds and models to create custom implants. Devices such as tissue engineered heart valves, artificial mandibles [13], composite hemi-knee joints [14], and cranioplasty prostheses [15] have been prepared using stereolithography.

The production of 3D scaffolds with well-controlled architecture at the micrometer-scale is a fundamental issue for the advancement of tissue engineering towards applications in health care. Stereolithography is a highly versatile and accurate technology to fabricate 3D scaffolds with controlled architectures [16], [17].

The scaffold is a support pattern that has to allow cell adhesion and direct the formation of tissue, therefore the architecture of its inner pore network and its outer geometry need to be well-defined. Without any three-dimensional supporting structures the cells will form a random two-dimensional mainly monolayer of cells.

The really important effect of scaffold pore network architecture on tissue (re)generation has been proved. Interconnecting pores enable supply of nutrients and metabolites as well as cell in growth; the correct pore size for a scaffold depends on the application but usually should be in the range of 5-10 times of the cell diameter (100-300 μm).

This approach is particularly important in bone tissue engineering since natural bone itself is a porous tissue. Indeed, almost all the ceramic scaffolds realized with stereolithography are limited to bone tissue engineering [18].

However it should be noted that recent research efforts have focused on developing elastic networks for soft tissue engineering applications.

Schuller-Ravoo et al., for example, investigated the applicability of flexible and elastic poly- (trimethylene carbonate) (PTMC) structures prepared by stereolithography as scaffolds for cartilage tissue engineering [19].

Encapsulation of cells, production of microenvironments mimicking the extracellular matrix, and fabrication of scaffolds with patterned arrays of biological materials are only some of the applications in which photocrosslinkble hydrogel can be used. In addition, they may be used for evaluating cell behaviour inside complex 3D microenvironments in order to obtain greater understanding of tissue and organ function [20].

Despite the great characteristics that the technology offers, the limited choice of photopolymerizable and biocompatible liquid polymer material is a problem that has to be dealt with.

Stereolithography requires, the use of a liquid photo-sensitive formulation that solidifies upon illumination. In tissue engineering applications, for example, the material from which the scaffold is prepared must have an appropriate rate of degradation in order to allow the surrounding tissue eventually replace the scaffold and the degradation products to not accumulate in the body and become cytotoxic. Limiting factors of this kind of technique are, therefore, the required post-processing steps and the stability of the structures over time.

In many cases, the printed object needs to be cleaned and support structures are usually manually removed. Many researches are developed in order to discover new materials that meet these characteristics and fit this specific manufacturing process.

Another criticism about stereolithography is the expense of printer maintenance and required peripherals. The machines themselves usually cost around $250.000. For this reason, it is uncommon to find stereolithography machines anywhere but in large companies or research group.

Digital Light Processing (DLP)

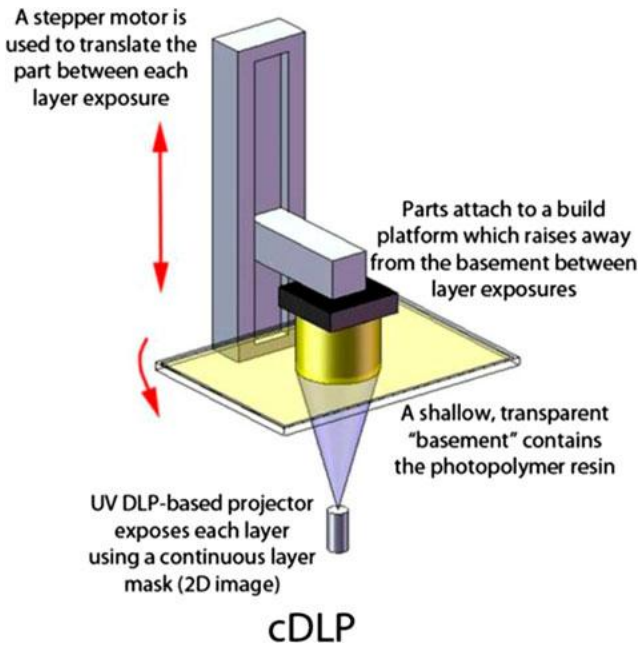

Figure 3 Schematic of a continuous Digital Light Processing system [21]

Digital light processing, called also micro-stereolithography or continuous digital light processing, was developed in 1987 by Texas Instrument. The key technology of this kind of technique is the interaction between a light source, that can be a laser or a projector, and a digital mirror device (DMD). The UV light shines on the DMD and it is then reflected on a photopolymer that cures after the exposition to the light following the basic principle of the stereolithography procedure (Fig. 3). The combination of a projector and a digital mirror device is called DLP projector.

The digital light processing printers prefer to use a top-down approach, starting to print the structures from the top rather than from the bottom. They utilize a tank to hold the resin and the build platform lowers down to extract the structure out of it. Beneath the resin tank there is a high definition DLP projector along with all the necessary circuit board to run. The projector projects images up to the bottom of the vat to cure each layer of resin. This will happen many hundreds or even thousands of times. After the curing process of the first structure's layer a peeling mechanism

separates it from the bottom of the vat and the build platform, to which the layer remains attached, moves up by one layer thickness. This happens for each layer and the different layers stick one below the other.

The layer's thickness can range from 5 μm up to more than 100 μm depending on the desired resolution on the Z-axis [22]. The exposure time for each layer is controlled with the software used to set up the printer. For most printers of this type the vat has a consumable duty special non-stick coating that allows the part to be peeled off more easily after each curing step. Each layer only needs a small amount of resin even for a large structure and is peeled using a servomotor that rotates and pulls the tank down gently peeling the part off from the bottom of it.

The main disadvantage of this kind of approach is that the structures, peeled off from the build plate after the illumination of each layer, are subjected to larger mechanical forces. But there are also a lot of advantages related to this technique in respect to the bottom-up systems: the surface being illuminated is always smooth, doesn't need post-processing of the structures, only small amounts of resin are required, and the illuminated layer is not exposed to the atmosphere, so oxygen inhibition is limited [17]. Besides, a DLP is constituted by less moving parts and has less stringent properties for the photopolymer material.

In stereolithography you can cure one pixel at the time as the laser crosses the layer, with DLP system instead you can process the entire area all at once. Traditionally lamps were used as light sources. Nowadays UV LEDs between 365 and 400-500 μm are the most common because of their high brightness capabilities, durability and long lifetime. Different materials require specific wavelengths to cure it. DMDs can work with the majority of the UV spectrum and this allows DLP printers to work with a wide range of materials and have a lot more of flexibility.

DMDs with special coatings for different UV wavelengths are also available. DLP printers use liquid photopolymer resin to build the object. Thank to DMDs an entire layer is exposed with the single pattern therefore fast print speeds are achievable regardless the layer complexity.

The DMD chip is an extremely precise light switch that enables light to be modulated digitally. This is made possible thanks to a rectangular array of

microscopic mirrors which is coordinated with a digital signal, a light source and a projection lens. The result is high picture brightness and contrast that are key component to the highest quality image.

These mirrors can reproduce graphics with incredible fidelity. DLP technology is famous for creating a clear and sharp picture by producing the exact mirror image of the source material being projected. The micromirrors of the DLP chip are less than a micron apart which means there are fewer gaps between pixels and projected images. Picture quality with DLP technology is also extremely reliable because DLP systems are based on digital instead of analog technology and because they reflect light instead of transmitting it so they are immune to the degradation that can occur by absorbing light. Optics are used to set the resolution on the image plane and intensity control LEDs adjust layer thickness resulting in finished parts that are smooth and accurate.

DLP technology brought a lot of advantages into the world of 3D printing and particularly in stereolithography. First of all, DMDs expose the entire layer in one shot which leads to improve throughput. DLP also has a faster build speed than point-by-point technologies and the printer speed is independent from design complexity as well as number of parts. High resolution DMDs are a cheap micro-level feature for high accuracy.

DLP technology is, therefore, an improved version of the conventional stereolithography and has the same applications into the different fields.

Lu et al. demonstrated not only that precisely controlled pore size and shapes can be easily fabricated in a scaffold for bone applications using a simple, computer-aided process, such as DLP but that is also possible to encapsulate cells in it during the procedure [23]. The feasibility of this technique is well-proved in literature and many efforts have been done to improve the process and the basic principles [21], [24], [25], [26].

The major drawback of this kind of technique is the cost. The cost of a DLP printer is much higher of that of a conventional SLA printer and this limits its use in the research environment.

Fused Deposition Modeling (FDM)

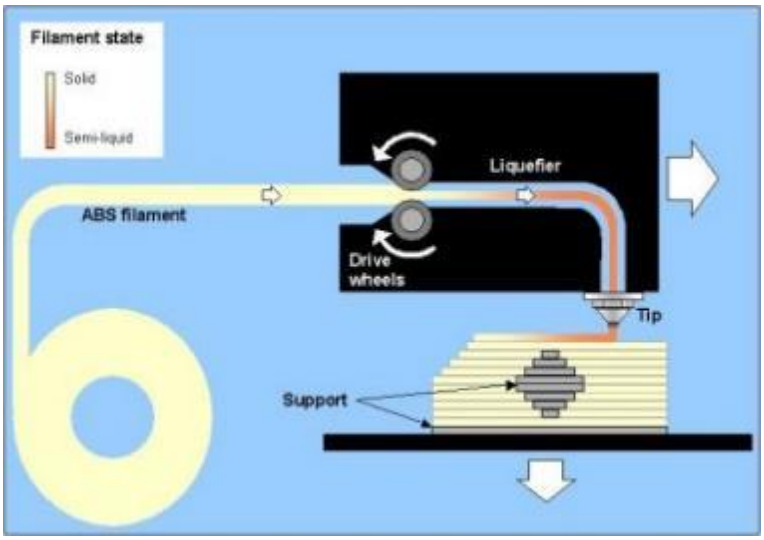

Figure 4 FDM system: the heated bed moves in longitudinal direction (z-axes), while the extruder moves in x and y axis [27]

Fused Deposition Modeling, or FDM, is a layer additive manufacturing process that uses production-grade thermoplastic materials to produce both prototype and end-use parts (Fig. 4).

The FDM was developed by Stratasys in the early 1990. This technology is known to accurately produce feature details and has an excellent strength-to-weight ratio. FDM is ideal for concept models, functional prototypes, manufacturing aids and low-volume end-use parts.

The FDM process begins by "slicing" 3D CAD data into layers. The data is then transferred to a machine which constructs the part layer by layer upon a build platform. Thin thread-like spools of thermoplastic and support material are used to create each cross-section of the part.

Similar to a hot melt glue gun, uncoiled material is slowly extruded through dual heated nozzles. The extrusion nozzles precisely lay down both support and thermoplastic material upon the preceding layers. The extrusion nozzle continues to move in a horizontal X-Y plane and while the build platform moves down, building the part layer by layer.

The finished part is removed from the build platform and cleaned of its support material. Raw FDM parts have visible layer lines. However, service providers offer multiple finishing options to create smooth, even surfaced parts including hand sanding, assembly and cosmetic paint.

Since FDM parts are constructed with production-grade thermoplastics (i.e. ABS, Polycarbonate and Ultem), they are both functional and durable. FDM is utilized in a number of industries including aerospace, automotive, industrial, commercial and medical.

In the medical field, FDM is used to realize prototype of anatomical structures (i.e. for the surgical planning phase), customized medical devices, such as external orthopaedic device (Fig. 5) or dental tools to fit individual anatomies. Moreover, FDM is used in tissue engineering that is one of the most important technique in biomedical field: it allows the formation of new viable tissue for a medical purpose, by using scaffold technology. FDM can be used to realize acellular scaffold and then allow the growth of a new tissue.

Figure 5 3D printed orthopedic device

The FDM process starts with the implementation of a CAD project, by design the desired structure. Then the process requires an export and transformation phase, because of the 3D printing machine can “comprise” only its “machine language format”: from .CAD file, a .stl extension is used (and also .slc and .sml sometimes; it depends on the software utilized). Then, the project is converted in G-Code, a numerical control programming language that allows the control of the stepper motor of the extruder in order to reach the correct position of the nozzle.

The FDM method forms three-dimensional objects from computer generated solid or surface models. Models can also be derived from computer tomography scans, magnetic resonance imaging scans, not only from model data created from 3D object digitizing systems.

FDM uses a small temperature controlled extruder to force out a thermoplastic filament material and deposit the semi-molten polymer onto a platform in a layer-by-layer process. The monofilament is moved by two rollers and acts as a piston to drive the semi-molten extrudate. At the end of each finished layer, the base platform is lowered and the next layer is deposited. The deposition path and parameters for every layer are designated depending on the material used, the fabrication conditions, the applications of the designed part and the preferences of the operator.

It is necessary to define some parameters in order to achieve a good result (i.e. the FDM head speed, the roller speed, the slice interval, and the direction of deposition within each layer).

The FDM technology can be used a lot in the biomedical field, and in particular in tissue engineering applications. For example, S.H. Masood et al. have studied different scaffold shapes and geometry, and then different probes of them have been realized, by using FDM method [28].

M.H Too et al. investigating the FDM viability in the fabrication of scaffolds, have found out that the process is highly capable of providing good control and reproducibility of the desired part geometry, degree of porosity and microstructure [29]. The high influence exerted by the FDM process parameters on the part microstructure, offers the user flexibility and ease of varying the structural characteristics of built parts to meet specific structural and functional requirements of scaffold.

FDM is utilized also in other field of medicine, like the cranial implants: G. Steven et al. have implanted a device realized by using FDM method, based on a model from a CT scan [30];

E. Kouhi et al. utilize FDM technology in reconstructive mandibular surgery [31].

Ning Xu et al. have investigated and realized a new type of artificial bones that mimic natural bones [32]. In this study, computed tomography (CT)-guided fused

deposition modeling (FDM) was employed to fabricate artificial bones. The in vitro mechanical properties, in vitro cell biocompatibility, and in vivo performance of the artificial bones were studied. All of the results indicate that CT-guided FDM is a simple, convenient, relatively low-cost method that is suitable for fabricating natural bonelike artificial bones.

The simplicity, reliability, and affordability of the FDM process have made the additive manufacturing technology widely recognized and adopted by industry, academia, and consumers. The FDM process has also been widely used by research and development sectors to improve the process, develop new materials, in a wide range of engineering applications.

The strengths of FDM are its capability to fabricate functional parts, ease of use, no need for supervision, flexibility and reproducibility. The cost of this method is very low. The time to produce parts, once the virtual model is available, will be fast and can be measured in terms of hours. Thus new products can be released with a markedly reduced time to market. Nevertheless, this technology is limited by a restricted accuracy (around 100 μm) and poor surface roughness [33]. These weaknesses can be explained by computer and mechanical aspects: the former is related to the approximation involved in surface tessellation and virtual model slicing; the latter regards the positioning error and the filament solidification problems, such as unpredictable shrinkage which causes part warping.

The resolution is lower with respect to other 3D printing technique: it was determined that accuracy and precision in the y direction (0.08-0.30 mm) are generally greater than in the x direction (0.12-0.62 mm) and the z direction (0.21-0.57 mm) [34].

Other drawbacks are the elevated temperature during the printing process and a small range of available materials.

In conclusion, the Fused Deposition Modeling method represents one of the most important development in the scientific and industrial field, thanks to the several advantages of this technique, even if some improvement could be necessary, in order to achieve an optimum trade-off between performances and costs.

Direct Ink Writing (DIW)

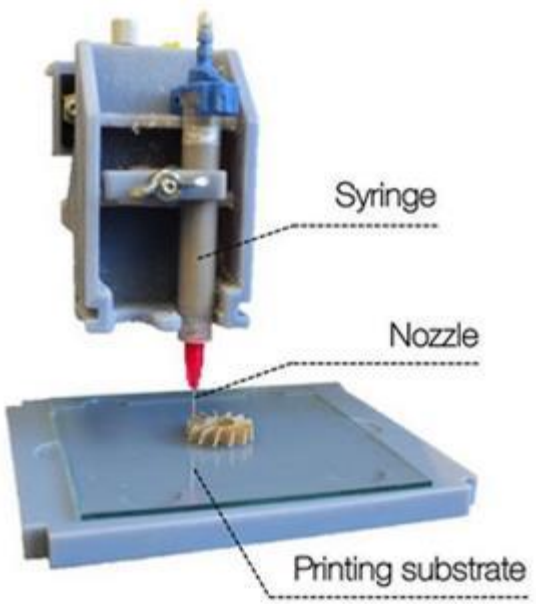

Figure 6 Direct Ink Writing technique: moving stage with syringe [35]

The definition “direct ink writing” describes fabrication methods based on a translation stage (controlled by computer), which moves an ink-deposition nozzle, in order to create materials with defined architecture and composition (Fig. 6).
The term “direct ink writing” was developed around the 1996 in the United States.
Direct ink writing (DIW) fabrication techniques allows one to design and rapidly fabricate materials in complex 3D shapes without the need for dies, lithographic masks, or expensive tools, which will simplify the process of material preparation and realize the product integrated manufacture. Compared with all the other solid freeform fabrication technologies, such as stereolithography, DIW can produce a 3D architecture at **room temperature** without any laser or ultraviolet light. Complex 3D architectures such as structures with high aspect ratio walls can be constructed in a layer-by-layer build sequence. Both the shape and the composition of micro zone can be controlled in each individual layer with various materials. Therefore, DIW has a

potential application value in the fabrication of catalytic materials, tissue engineering scaffolds [36] and piezoelectric composites [37].

Different direct ink writing techniques have been introduced and they can be divided into two different "big families" [38]: filament-based approaches and droplet-based approaches.

DIW filament-based techniques are: robocasting (or robotic deposition), micro-pen writing, and fused deposition.

They have some similarity with FDM techniques: both the technologies start from a CAD project, converted in .stl file and then in G-code. The printing machine can moves its nozzle in the work space and realize the structure. The DIW filament-based technology and the FDM possess the same electronic and mechanical elements that manage the handling dynamics of the extruder head. In both of them, the material that has to be deposited is extruded as a continuous filament through a nozzle, whose diameter can vary from some hundreds of microns and determines the lateral resolution of the system. The nozzle area, the velocity at which the material is pushed and its density determine the flow rate and hence the speed and the deposition flux.

The main difference between DIW filament-based technology and FDM is in the material used: in DIW filament-based technology, a liquid ink, usually a highly viscous colloidal gel, is utilized, while in FDM method a thermoplastic-based material is heated and printed.

For filament-based techniques, there are two types of ink delivery systems [39]: constant-displacement and constant-pressure extrusion. In constant-displacement techniques, the filament extrusion is achieved by mechanically displacing the plunger of the ink reservoir at the pressure required to maintain the desired flow conditions. In constant-pressure writing, instead, ink filaments are extruded by applying a uniform pressure to the reservoir. This approach is less common as slight variations in rheological properties induce fluctuations in the volumetric flow rate [40].

DIW droplet-based techniques, instead, are: 3D printing (3DP), direct ink-jet printing and hot-melt printing.

For this kind of DIW techniques, two main types of delivery systems exist: the continuous and the droplet-on-demand ink-jet printing [41].

The ink-jet printing system delivers reproducible, uniform droplets with a fixed volume from a single or multi-array nozzle. The printer heads are usually piezo-electric [42]; by varying the voltage, it is possible to change the applied pressure inside the print head and eject the droplets. The shape of the droplets depends on the size of the nozzle and on the ink rheology. Really important is the role played by the fluid dynamics involved in the droplets formation.

The continuous ink-jet printing technique operates in a continuous stream mode and utilizes electrically conducting fluid that can be steered by applying an electrostatic field. This allows to build structures with really high speed but lacks high quality printing. The droplet-on-demand instead provides high resolute structures; individual droplets of ink are extruded from small diameter vessels directly on a specified position of the substrate only when required. In Fig. 7, a block diagram of all the different kind of DIW techniques is presented.

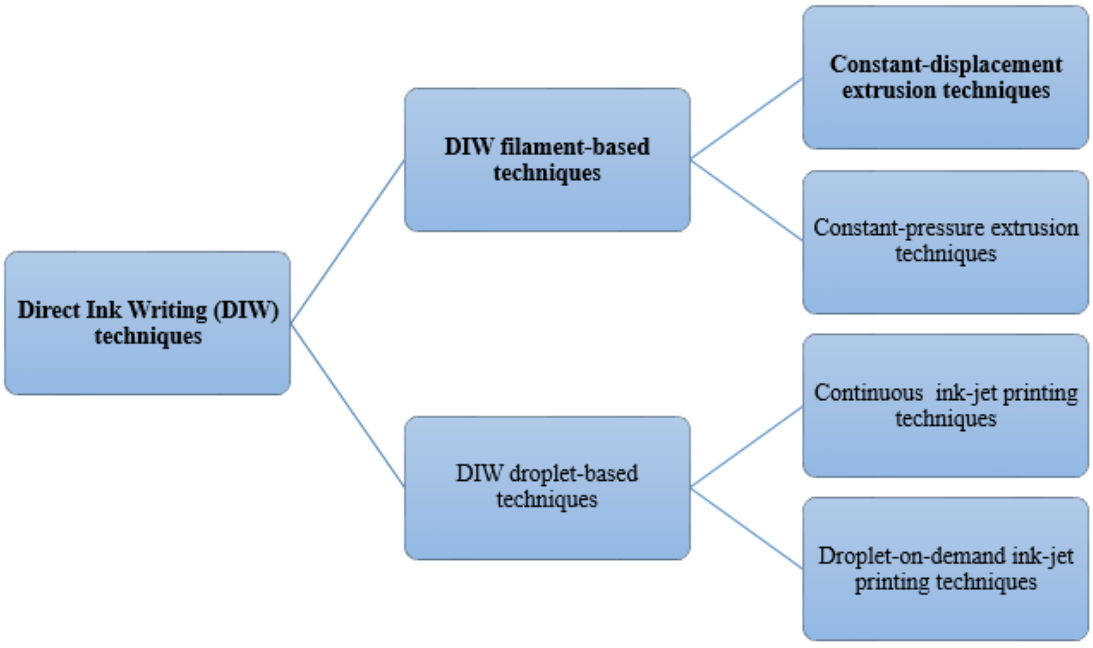

Figure 7 Block diagram of the different DIW techniques. In bold it is highlighted the kind of technique for which the deposition system, presented in the next chapter, was optimized.

The main challenges in DIW filament-based and droplet-based techniques are therefore the ink design, the characterization of its dynamics during deposition and the optimization of the ink-delivery system to achieve precise structures and tailored products. The use of the DIW droplet-based techniques for the realization of 3D objects is limited due to the fact that these kind of techniques use slightly viscous solution to print the structure. Little viscous solutions have an impact on the printed structure layer's height which often does not allow to realize real 3D structures (< 1 μm). The major advantage of DIW filament-based techniques compared to the droplet-based is therefore that with filament-based techniques is possible to fabricated higher structures with a better control on the single layer's thickness.

In any case, the possibility to specifically control the composition and the structure of the printed material at micrometre level open a broad range of possible technological applications for both the DIW techniques. The low cost of the instrumentation also contributes, with the flexibility and the continuous design of new materials, to set a boundary line between the techniques used so far and the new generation of the 3D printing technology.

Jennifer A. Lewis, co-Director at Harvard University, is one of the greatest exponents of 3D printing (direct-ink-writing) worldwide. She and her collaborators, starting from the analysis of the properties of the materials and the understanding of the basic principles of the involved system, have exacerbated this concept taking it at the best level so far in all fields of application. The Lewis Lab focuses on the programmable assembly of soft materials. Specifically, they design and fabricate functional, structural and biological materials with controlled composition and architecture across multiple length scales. Architected soft matter may find potential application as electronics, optical materials, lightweight structures, and 3D vascularized tissues.

Numerous works of the Lewis lab in the biomedical field and in particular referred to the study of the correct properties of the materials involved in DIW filament-based technology were analysed as considered during this thesis project as a support and a foundation of the developed theories.

The aim of the project was, indeed, to characterize and optimize a commercial 3D printer for controlled extrusion of hydrogels knowing the basic principles of the DIW filament-based techniques, as shown from the Fig.7. The understanding of the interaction between the deposition system and the material used has proved to be so crucial for the analysis of the obtained results and the development of the final conclusions and the future perspectives.

In the table below are shown the main differences in terms of resolution, advantages, disadvantages and suitability for tissue engineering applications between the four kinds of 3D printing technologies evaluated so far

Table 1 Comparison of different rapid prototyping (RP) methods

RP technique	Vertical Resolution (µm)	Advantages	Disadvantages	Suitability in tissue engineering	Ref.
Stereolithography (SLA)	25 - 200 µm	High resolution and accuracy, possibility to achieve exquisite details.	Limited choice of materials, high costs, required post-processing, stability of the structures over time.	Mainly used for a-cellular 3D scaffolds (non-fully biocompatibility of the crosslinking process).	[16] [17] [19] [20]
Digital Light Processing (DLP)	5 – 100 µm	Higher resolution, smooth surfaces, no need of post-processing, no oxygen inhibition, faster build speed.	Larger mechanical forces, higher costs, limited choice of materials.	Mainly used for a-cellular 3D scaffolds (non-fully biocompatibility of the crosslinking process).	[21] [22] [23] [24] [25]
Fused Deposition Modelling (FDM)	100 - 250 µm	Low costs, easy-to-use.	Restricted accuracy and resolution, poor surface roughness, small range of materials, use of elevated temperatures.	Used for a-cellular 3D scaffolds (non biocompatibility of the process).	[29] [31] [33] [34] [43] [44]
Direct Ink Writing (DIW) techniques	0.1 µm	Materials flexibility, low cost and ability to construct arbitrary 3D structures with any size or shape.	Limited choice of materials and size, negligible mechanical properties	Used for both a-cellular scaffolds and bioprinted ones.	[38] [39] [41] [42]

CHAPTER 3
DEPOSITION SYSTEM

From the very start the 3D printing has been about bringing innovations that can turn people life around and as a result 3D bioprinting technology has changed the world. Thanks to the helpful collaboration provided by the Bioanalytics group of the DTU's (Denmark Technological University) Nanotech department, it was possible to set up a system for controlled extrusion of hydrogels. It is composed by a **3D printer** for fused deposition modelling and a simple system, called **paste extruder**, that allows the outflow of the fluid by a controlled pressure on the piston of a syringe. Many optimizations, from the fabrication of holders that allow the use of different syringes to the design of a new nozzle, have been presented. In this chapter, all the equipment and the techniques used during this thesis project will be showed and described. All the basic laws that form the foundation of the used system will be demonstrated and justified.

Mechanical Set-Up

The system used during the project is composed by two main parts: a computer-controlled 3D printer and a paste extruder (the Discov3ry) electrically connected to the printer. The paste extruder serves as a feeder for the 3D printer. It controls the movement of the syringe cartridge which conveys the fluid into the tip mounted on the 3D printer head (Fig. 8).

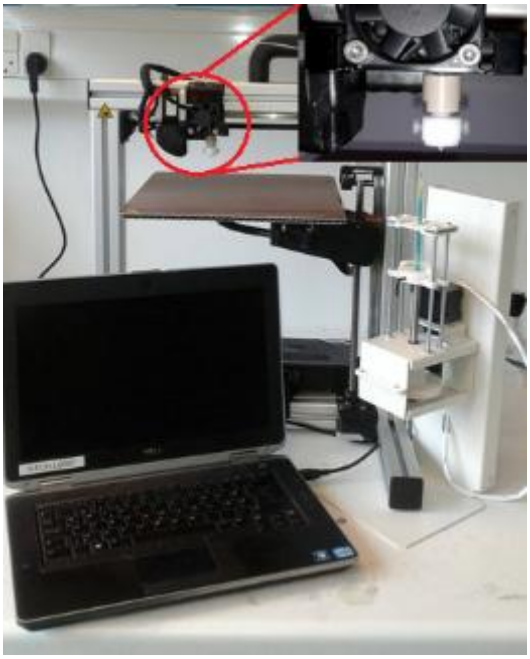

Figure 8 Mechanical set-up used during the project. From the left: the computer, the 3D printer and the paste extruder

The experimental tests have highlighted two problems:

1. The non-perfect control of the amount of material extruded per unit of time (**flow rate**).
2. The mechanical deficiencies of the holder of the tip assembled on the printer head.

Regarding the latter, we wanted a way to easily calibrate the tip of the paste extruder without compromising the Z-axis movement capabilities. We decided therefore for the fabrication of a customized tip holder. The final holder made was inspired by the design of the 3D printer hot-end but it is important to remark that the fluid is not heated in the tip on in any other part of the paste extruder system that allows only cold extrusion.

A complete overview of the two components utilized (the 3D printer, its main components, its hot-end, its extruder and the Discov3ry) is then provided. The understanding of the parallelism between the design of the holder of the tip and the hot-end of the 3D printer and the use of the Discov3ry instead of the extruder of the printer, it is relevant to solve the two cited problems.

The Felix 3.0 Dual Extruder 3D printer

Figure 9 The Felix 3.0 Dual Extruder [45]

The 3D printer is a Felix 3.0 dual extruder made by Felix Printers (Fig. 9). The Felix 3.0 can be connected, through a USB cable, to a computer or can be directly controlled through a LCD screen placed just at the base of the printer and can print with a standalone microSD card.

The control board is an Arduino based (atmega 2560) working at 12V innovatively designed by the company, able to drive 5 stepper motors (3 for the movements along the XYZ axis and 1 for each extruder; all of them are bipolar stepper motors Nema 17), 3 high power heaters (a 144W bed heater, one 30 W heater cartridge for each extruder) and several other I/O's. All without the need of active cooling.

The three stepper motors that control the movements along the three axis X, Y and Z allow to have a positioning resolution of 13 μm along X and Y and of 0.4 μm along Z.

The circuitry is embedded in a rigid aluminium frame that supports the whole design.

The printing process starts by loading a plastic filament into the 3D printer which needs to be processed using the two core parts of the printer: its extruder and its hot-end (Fig. 10). The extruder and the hot-end are two distinct parts: the part that pushes the plastic filament is the extruder, the feeder; the hot-end, instead, is the part that melts the plastic material and provides a fine filament for the nozzle. The hot-end is strapped right to the extruder. The extruder is based on a drive filament gear in contact with the extruder's stepper motor and this is useful to produce the right grip on the filament. The drive filament gear or the extruder drive wheel, as it called, is made of strong material that results in a high level of durability. The perfectly shaped

teeth prevent the wheel from losing grip when pulling in the filament.
This tension system allows to control how much tension you put on the filament. In order to use it there is a little hex screw on the top of the extruder and by turning it counter clockwise, you can actually put more tension on the filament.
The hot-end of the Felix 3.0 is composed by four part: the base, the peek isolation element, the heater barrel and the nozzle.

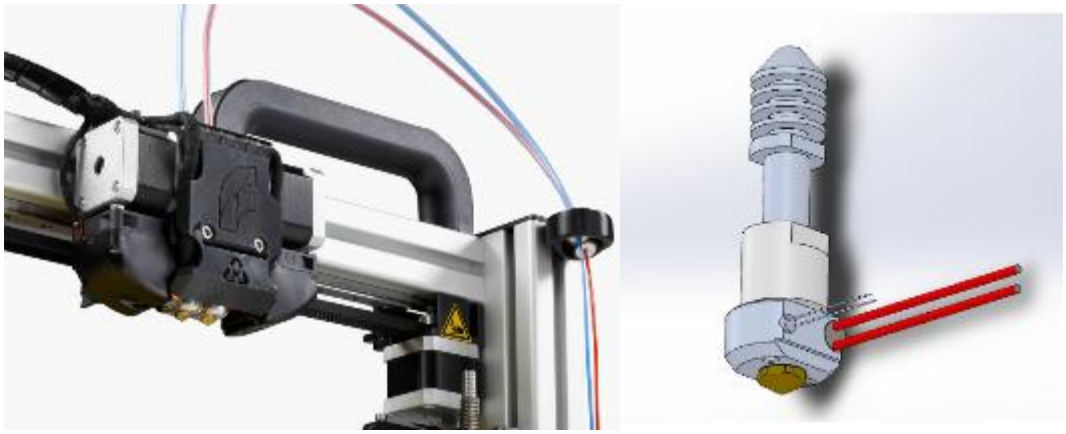

Figure 10 Left: Extruder – Hot-end system; Right: Design of the 3D printer hot-end. From the top to the bottom: base, peek isolation element, heater barrel and the nozzle [45]

The base is the top part of the hot-end; cooling ribs are designed onto the base to maintain an excellent heat balance in different circumstances. It features as a shaft for the filament to be heated and become liquid. The hot-end peek isolation part is used to keep the heat in the lower part of the hot-end and to keep the upper part of the hot-end cool in order to avoid sudden temperature changes. The hot-end heated barrel transmits heat from the heater part to the filament and it also provides space for a heater and a temperature sensor. All the presented components are made for filament having a diameter of 1.75mm with a high quality aluminium. The hot-end nozzle is the part where the filament leaves the extruder. The diameter of this nozzle can be 0.35 mm or 0.5 mm. The tip is made out of brass to ensure constant and reliable performances.
The build plate on this printer is massive. A horizontal level build plate is very important for the first layer to attach. It consists of a 6mm thick sandwich aluminium plate (25, 5 x 20, 5 x 22 cm). The 3-point manual bed levelling system makes is easy to level the build plate and this ensures optimal adhesion of objects to the print

surface. The plate is covered with one piece of Kapton tape to avoid sticking pieces on top of it. Two aspects are really interesting in this kind of 3D printer: the design of the hot-end that makes it easy to calibrate and the possibility to obtain an even heat distribution throughout the entire plate (the deviation of temp over the whole bed is less than 0.5 degC at 60degC).

The Discov3ry universal paste extruder

The Discov3ry is a paste extruder made by the Structur3D printing that can be easily connected to almost any kind of 3D printer thanks to a pre-integrated electronics (4 stepper motor leads). The term “paste extruder” is due to fact that the system combines the power and precision of a 3D Printer for FDM (“extruder”) with a broad range of materials, from silicone to plastic to bio-materials (“paste”). The Discov3ry (dimensions: 6" x 6" x 14", weight: 10 lbs) allows to dispense a soft material forcing the paste through a feed tube and extruding it with a tip mounted to the 3D printer head.

Figure 11 The Discov3ry universal paste extruder

The integrated system is composed by (Fig. 11):

- A bipolar stepper motor 42STH38-168A4B-2 electrically connected to the 3D printer as one of the two extruders;
- A planetary gearbox 36JXS60KS1G connected to the motor;
- A plastic gear wheel;
- An endless screw fixed to the base of the syringe cartridge.

The planetary gearbox on the motor has a gear ratio of 51:1.

When a gear is connected to a power source, like an electric motor, then it is called the **driver gear**. The gear to which is matched is called the **driven gear**. The ratio of the number of revolutions of the driver gear to the number of revolutions of the driven gear is called the **gear ratio** (Fig. 12). The larger is the gear ratio the slower the driven gear will turn in relation to the driver gear speed (in the case of the planetary gearbox for 51 rotations of the stepper motor the gear box does 1). At the same time, the torque applied to the driven gear will be greater than that applied to the driver gear by a factor equal to the gear ratio (the torque of the planetary gearbox is 51 times greater than that of the stepper motor).

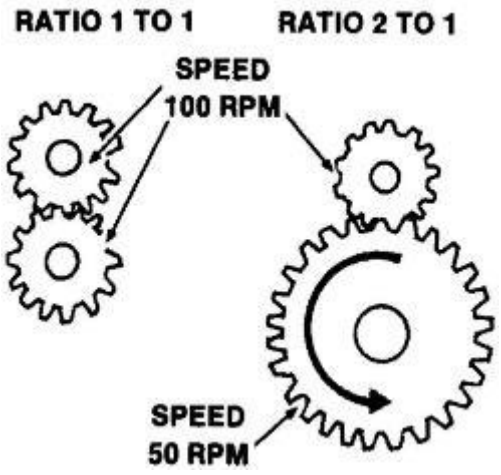

Figure 12 Schematic describing the concept of the gear ratio. The gear on top is the driver gear, the other one is the driven gear [67]

The system uses also an internal gearbox ratio, due to the mechanical connection between the gearbox (driver gear) and the plastic gear wheel (driven gear), of 5:1. This brings the overall gear ratio of the Discov3ry to 255:1 (stepper motor-plastic gear wheel).

The Discov3ry is fabricated for locking syringes of 60cc. In order to print with only small quantity of the protein solution used during the project, different holders of different sizes (1ml syringe, 5ml syringe) were fabricated using the Felix 3.0 dual extruder. In the attachment A, there are the designs made in SolidWorks of them.

Calibration of the System

Correct nozzle height and bed levelling are the two most important factors in 3D printing. This makes a huge difference to the reliability of the print and between a successful print and an unsuccessful one. It is really important that the table is properly calibrated: the distance between the nozzle and the table should be the same at every x-y position. Errors in this calibration amount to most of failed prints. The hot-ends, in a dual extruder 3D printer, should also be at the same height with respect to the just levelled heated bed.

It is always essential to level the bed first. To do so, with a Felix 3.0 dual extruder, there are three M4 nuts underneath the heated bed that mark the three adjustment points to calibrate. It is also useful to have a plain piece of paper that is usually around 70 μm thick, which is ideal for this kind of task.

The procedure includes three steps and starts by setting the nuts at the centre of their adjustment range and heating up the nozzle and the bed in order to calibrate the printer when it is in the same conditions as when it is working. The second step is to move or slide the hot-end over to the center of the bed (Fig. 13). While the third and last one is to set the end-stop of the printer's Z-axis as the point where the nozzle starts exerting a little pressure on the paper sheet. It is necessary to lift the nozzle and repeat these steps for each adjustment point around the bed. At the end of the procedure, the nozzle and the bed will have an uniform distance of 50-70 μm between them that doesn't allow the nozzle either to scratch on the surface of the build plate or to be too far away from it.

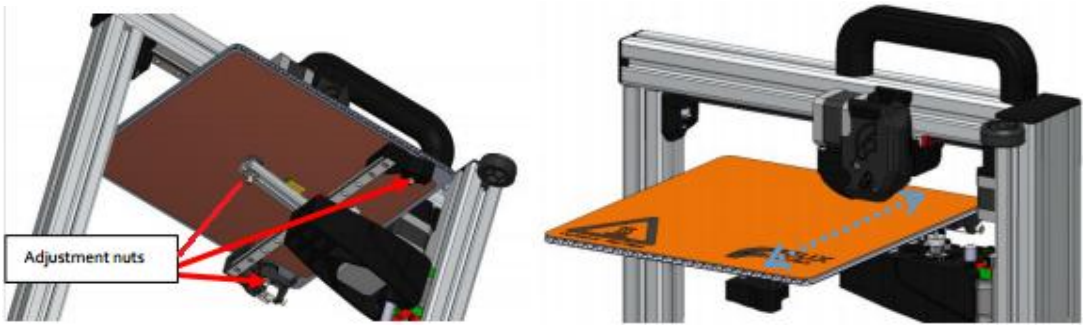

Figure 13 Schematic illustration of the first two calibration steps [46]

Once the bed is correctly levelled, it will possible to adjust the correct height of the two hot-ends fastening the M4x12 bolds place at the bottom of the plastic case containing both the extruders and the hot-ends (Fig. 14).

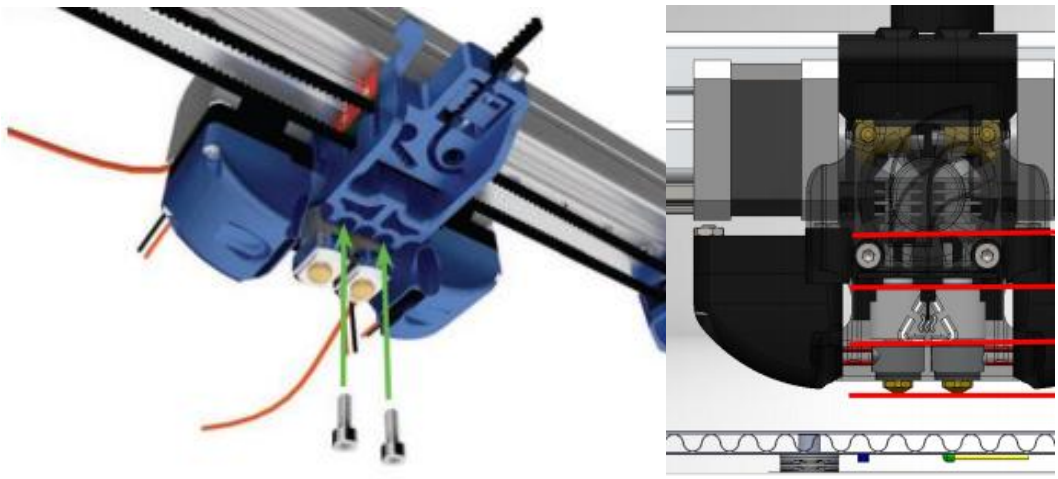

Figure 14 Calibration of the two hot ends in respect to the levelled build plate [46]

Thus to achieve a correct calibration of the whole system is really important that the hot-ends are fixed and stable in respect to the bed and that it is possible to move them one in respect to the other.

A great problem was, therefore, to design a holder for the tip of the Discov3ry that was not only possible to assemble on the 3D printer head but that would allow stability and the possibility of movements along the Z-axis.

Three generations of the tip's holder are presented.

The first one, in Fig. 15 on the left, was the holder sent from the company with the Discov3ry. It is a single plastic piece designed for a large feed tube that fitted a syringe of 60cc. The tip of the Discov3ry resulted not stable; it was continuously shaking during the print and there was no possibility to change its position along the Z-axis.

The second generation, represented in centre of the Fig. 15, was designed with SolidWorks and 3D printed with the Felix 3.0 dual extruder in PLA. It is composed by two different parts: the support part and the movable one. The support part was fixed by two M4x40 screws to the head of the 3D printer. It showed a 7 mm rectangular hole in the bottom part that allowed it to finely adjust the position of the

movable part, and so of the tip, in respect to the printer's hot-end along the Z-axis, by screwing it with a M4 nut. Once found the correct position, the movable part is fixed with respect the 3D printer head.

The movable part is basically a cylinder whose internal diameter is set, with some tolerance, on the feed tube external diameter in order to tight the tube, with the tip in it, in a fixed position. The problem of this kind of holder was that the movable part was in plastic, so achieving a good grip on the system tube-tip was not possible, even if the internal diameter of the part (external diameter of the tube only) was smaller than that of the combination tube-tip. In attachment A, there is the whole design (support and movable part) of the second generation holder.

The third generation, Fig. 15 on the right, is the most recent one and it allows to achieve a good stability and the possibility to calibrate perfectly the tip along the Z-axis. The components of the holder are the same of the Felix 3.0 dual extruder's hot-end, apart from the nozzle that in this case is the tip of the syringe and the hot-end heated barrel that it is made in Teflon and has two M4 screws on the sides, also fabricated in Teflon, to slightly tight the tip of the syringe making it stable. The other difference is that the barrel cannot be heated because it does not provide space for a heater and a thermistor like the previous one; but in case this is necessary it can be easily redesigned for this purpose. Because the final shape of the holder is the same of the printer's hot-ends, it is possible to adjust the position of the tip along the Z-axis in the same way we have seen before for them. This is really important because allows to calibrate the stage correctly and open the possibility to use two different kind of "extruder" and print both with liquid and plastic at the same time.

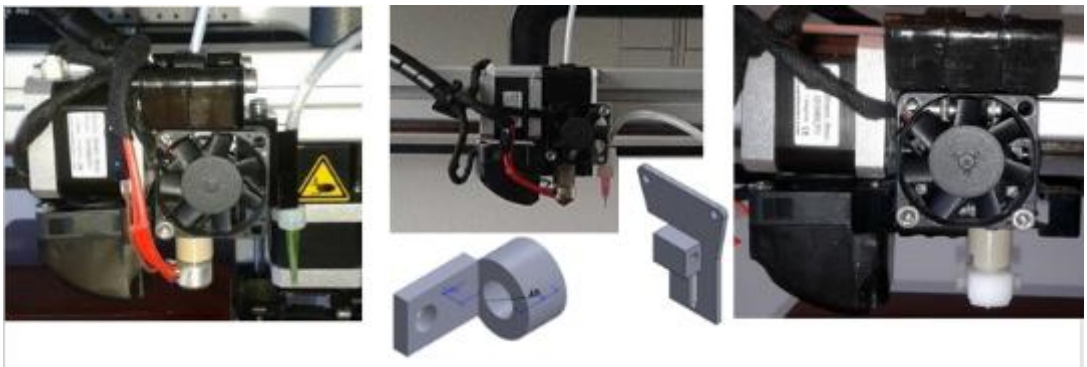

Figure 15 The three generations of the tip's holder. Starting from the left: the first, the second and the third one.

Model of the system

The printing precision is primarily based on the precise control of the flow rate that is the amount of material that is extruded per time. This can be achieved thanks to the understanding of the basic principles governing the new extrusion system. The Discov3ry behaves like a syringe pump. It consists in a simple source of linear motion that controls the speed at which the piston is driven. By fixing the rotational frequency of the stepper motor and knowing the overall gear ratio, it is possible to determine the angular speed of the Discov3ry's gear wheel (Θ) $\left[\frac{rad}{s}\right]$ and the linear speed (S) of the endless screw $\left[\frac{mm}{s}\right]$ with the following formula [47]:

$$S = \frac{np\Theta}{2\pi}$$

Where n and p are respectively the number of principles and the pitch of the screw [mm]. The motion of the coupling screw-nut is helical; the nut (white gear wheel) rotates while the screw, fixed to the base that houses the plunger of the syringe with an Allen key, can only shift. For the screw of the Discov3ry n is equal to 1 and a pitch (p) of 2.53mm has been measured.

If the syringe's diameter is known, it is possible to achieve the desired flow rate adapting the linear speed of the screw, and so that of the piston of the syringe, following this formula (continuity equation for incompressible fluids):

$$Q = S\phi$$

Where Q is the flow rate $\left[\frac{mm^3}{s}\right]$, S is the linear speed of the piston $\left[\frac{mm}{s}\right]$ and ϕ is the cross-sectional area of the syringe $[mm^2]$.

The equation expresses the concept that the mass of fluid entering from one end of a pipe must exit from the other one if in the stretch considered it does not occur revenue or outlets of the fluid.

A syringe pump is mainly characterized by its settling time.

The settling time of a syringe pump depends not only on the quality of its mechanics, but also, and more importantly, on the fluidic resistance (R) and the fluidic compliance (C) of the experimental setup, having a lot to do with the compression characteristics of the material, along with flow resistance through the tubing.

If we change the flow rate (Q), the piston pushes the syringe, increasing the pressure in the fluidic system and deforming it instead of putting the liquid into motion. The system, therefore, is designed to slowly build up pressure based on the relationship between flow resistance, fluid compression, and motor power. Eventually, the pressure reaches a cutover point, when it overcomes the flow resistance, and causes the material to move through the tubing and out of the nozzle. From that point on, the system incrementally moves the lead screw upward to continually keep the pressure at that steady state.

Depending on the fluidic resistance and elasticity of the system, the settling time can change from a hundredth of ms in a rigid fluidic system with a low resistance to hours for a soft fluidic system with a very high fluidic resistance. It is crucial when dealing with syringe pumps to get an estimation of the responsiveness of the flow rate in the experimental conditions. Knowing the properties of the material and the characteristics of the system, it is possible to calculate the settling time [s] of the Discov3ry with the following formula:

$$\tau = R\ C$$

Where R is the fluidic resistance (Poiseuille's law for Newtonian fluid and cylindrical pipes):

$$R = \frac{8\mu L}{\pi r^4}$$

- μ [Pa s]: fluid viscosity;
- L [m]: length of the pipe;
- r [m]: radius of the pipe.

And C is the fluidic compliance (for cylindrical tanks):

$$C = \frac{A}{\rho g}$$

- ρ $\left[\frac{kg}{m^3}\right]$: density of the fluid
- A $[m^2]$: cross-sectional area of the tank;
- g $\left[\frac{m}{s^2}\right]$: gravity acceleration.

In the Discov3ry's syringe-tube system, the fluidic compliance is determined by the syringe that has a greater cross-sectional area compared to the tube while, on the other hand, the fluidic resistance is given by the tube as it is definitely longer and has a lower radius. During the project, syringes of 1ml and 5ml (respectively with an internal diameter of 4.78mm and 12.05mm) and tubes with an inner diameter of 0.9mm and 0.5mm have been used.

How to control the flow rate

It is possible to check the correct amount of material that is extruded per time, the **flow rate**, in two ways: chancing the firmware's parameters that control the extruder motor (where is possible) or by intervening on the flow tweak. Both of the two approaches have been used to finely tune the flow rate of the Discov3ry. The firmware controls basically every aspect of a 3D printer from step control to heat management to the communication with the printer host; everything is handled by some parts of the firmware. The term "firmware" denotes the fixed programs that internally control various electronic devices. The Felix is configured so that it knows how many steps to generate for 1 mm of X motion, 1 mm of Y motion, 1 mm of Z motion and 1 mm of filament motion.

Once the computer is connected with the printer, it is possible to set these parameters in the firmware EEPROM Configuration and edit the standard ones for the extruders. Altering these values, you are able to let the stepper spin at any possible speed. In this case, it is useful to translate the values to microsteps per mm of motion of the Discov3ry plunger spindle.The Felix board uses 16 microsteps per step, so 3200 microsteps per revolution for the stepper of the Discov3ry, considering that it does

1.8° per step and 200 steps per revolution. So fixing the $\frac{steps}{mm}$ (SM) and setting the speed with which the material is extruded ($V_{extrusion}$) in $\frac{mm}{s}$, it is possible to calculate the rotational speed of the stepper motor (F) in Hz with the following formula:

$$F = \frac{SM * V_{extrusion}}{3200steps}$$

This result is very important because as seen during the descriptions of the basic principles that govern the system, knowing the overall gear ratio and the relationship that links the linear speed of the screw to the angular speed of the gear wheel, it is possible to change F to obtain the desired flow rate.

Most slicers do not do extensive calculations on flow rate. They simply use the "what goes in must come out" principle. Assuming that the extrusion does not stall, it is possible, known the speed at which we push filament in ($V_{extrusion}$) $\left[\frac{mm}{s}\right]$ and the diameter of the filament (d) [mm], to determine the amount of material extruded.

The needed volume depends, also, on material properties (the material shrinks when cooling down, for example), layer thickness (h) [mm], desired line width (w) [mm] and printer head's and build plate's speed (v_0) $\left[\frac{mm}{s}\right]$.

$$FT * h * w * v_0 = \frac{\pi d^2}{4} V_{extrusion}$$

The flow tweak (FT) is a setting parameter of the used slicing program: KISSlicer. It is normally used to compensate for the material's behaviour, in the case of the Discov3ry is used to compensate for the fact that we are printing with a liquid solution instead of with a plastic filament, and with a completely different extruding system. The diameter of the filament (d) has been set to 1mm.

A good slicer has also to take into account that the Discov3ry will not instantaneously extrude material at the desired speed, it will ramp up. Likewise, it

cannot stop extruding at once. Therefore two calibration lines must be printed in order to reach the steady state of the system as well as a good setting of the prime, suck and wipe parameters of the slicing program. A precisely control on the amount of extrusion and on the extrusion speed can eliminate a significant shear stress on the material that can impact cell viability. Major information about the software and all the main settings used during this thesis project can be found in attachment B.

CHAPTER 4
INK DESIGN

3D bioprinting opened new frontiers in the field of tissue engineering by introducing new limits and, overcoming these, consequently new goals. The biggest issue of this new technology is the design of new materials that prove to be not only biocompatible but also printable. The necessary features in order that a new ink is used in this area are described; the concepts of viscosity and rheological properties of the material are briefly introduced. The silk fibroin (SF) solution is a biocompatible material with extremely good properties for applications in tissue engineering, such as scaffolding. The main characteristics of this kind of solution are also presented.

3D Bioprinting: integrating Form and Function

Many efforts have been spent in tissue engineering to realize viable tissues and organs for transplantation. It is a very complex task due to the complexity of the tissue biology and until now only thin skin and avascular cartilage have been successfully fabricated. In this context, 3D bioprinting has opened new possibilities, allowing to realize personalized and precise structures shaped with tissue-like complexity using patient's own cells. Its aim is to achieve a really well-defined spatial distribution of cells, growth factors and biomaterials at the microscale level that characterize a tissue-like structure. Additive Manufacturing (AM) technologies, indeed, allow to realize very accurate and repeatable control of the scaffold geometry.

In order to generate a specific phenotype, the single cell changes its structure in accordance with every kind of stimulus that receives from the various components of the extracellular matrix (ECM) and from adjacent and even distant cells (Fig. 16). A particular challenge is the coupling of chemical and mechanical signals.

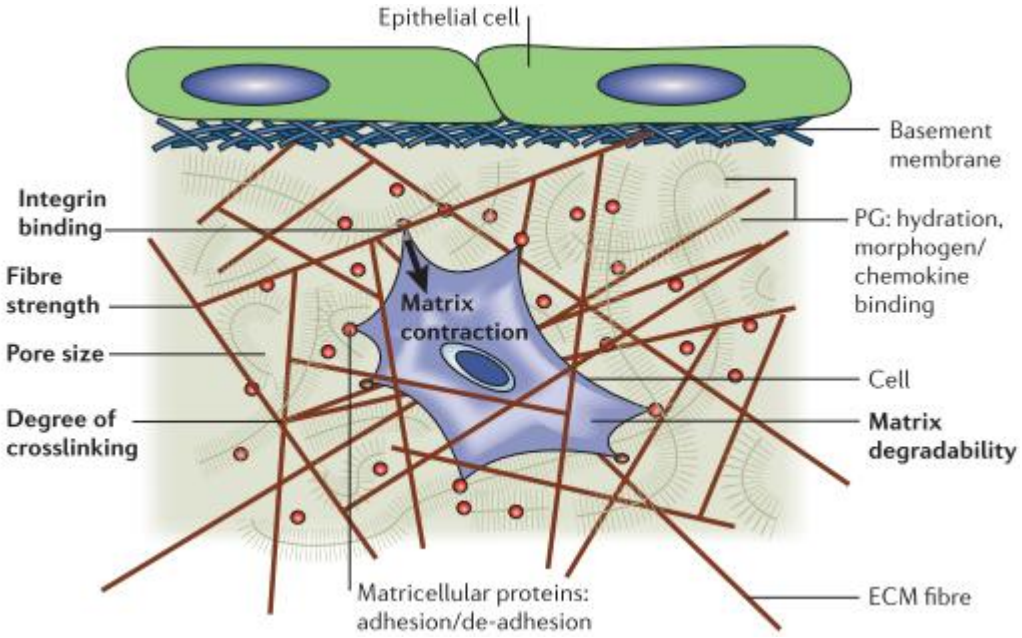

Figure 16 The importance of the 3D environment for engineering cell function [48]

In a 3D environment, tissue-scale solute concentration gradients and solute diffusion can be established as well as different external mechanical inputs that affect cell contraction and associated intracellular signalling; furthermore, the 3D environment might be necessary to model morphogenetic and remodelling events that occur over larger-length scales and realize structures constituted by layers with different properties and functions as it is in tissues [48]:
3D bioprinting is defined as:

> "The use of material transfer processes for patterning and assembling biologically relevant materials, molecules, cells, tissues, and biodegradable biomaterials with a prescribed organization to accomplish one or more biological functions [49]"

Different printing parameters, biomaterials and properties of the 3D-printed constructs have to be taken into considerations [50], [51]. In absence of cells, every efforts is dedicated to manufacture the scaffold and the biomaterial itself in less restrictive fabrication conditions with a resulting high accuracy and resolution and a great shape complexity. In 3D bioprinting, instead, it is necessary to maintain the cells and the other biological agents, presented into the material during manufacturing, alive in order to fabricate a living tissue constructs. A scaffold has to show appropriate mechanical and biochemical properties in order to mimic the extracellular matrix (ECM) and provide mechanical integrity. Biocompatibility and biodegradability are only some of the mechanical properties that have to be presented. The scaffold should not shrink or swell in order to have a controlled structure and should allow cell attachment. The porosity is another key feature for a scaffold; it facilitates tissue ingrowth and improves cell viability. The specific material selected to compose the scaffold has to recreate the nature of the engineered tissue and provides the right biochemical, biophysical, biomechanical, bioelectrical and biomagnetic signal. The printing material requires also a high water content, it has to be soft in terms of stiffness and biodegradable in order to allow cells spreading, migration and proliferation. A sufficient porosity of the material it is also necessary for the correct transport of nutrients and oxygen and for the correct

removal of the waste. An example of the construct usually fabricated in bioprinting applications is shown in Fig. 17.

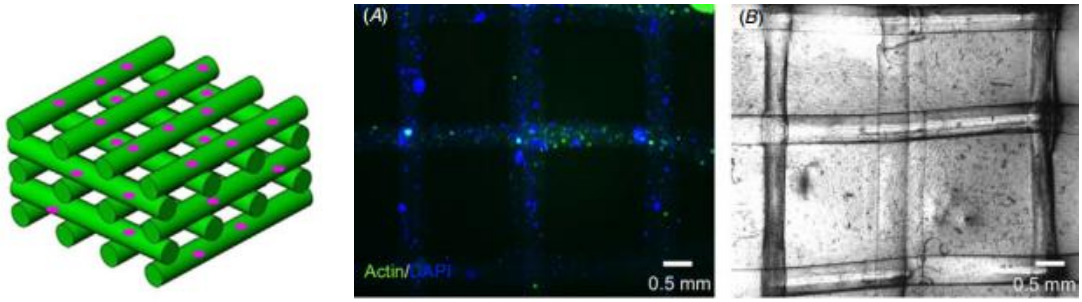

Figure 17 On the left: Representative image of a hydrogel cell-laden construct (green: lattice; fuchsia: cells) ; In the centre and on the right: (A) fluorescence image of a F-actin/DAPI stained two-layered lattice architecture bioprinted with HepG2-laden GelMA hydrogels, (B) representative brightfield image of lattice architecture shown in (A), (scale bar, 500 μm) [52].

However, sterile conditions, non-toxic materials, mild fabrication processes, and relatively short processing time windows are also required [53].

Printing a complete structure can take around 1- 2 hours and during this amount of time the cells in solution, that are usually heavier than water, start to set down to the bottom of the plate. So as a result there is not an even distribution of the cells in the final structure. In order to allow cells floating or suspension, it is possible to act on the density of the solution (equal to that of the cells) or on its viscosity (the cells are sticking in a sort of glue). Heterogeneous architecture and cell distributions can be achieved also by using multiple cell types and biomaterials with different properties.

The most used materials for this kind of applications are hydrogels due their similarity to the native ECM. Usually hydrogels need to have high viscosity not only to allow cells floating or suspension but also to hold the shape during and after extrusion. The extruded hydrogels are further cross-linked through various physical or chemical approaches to fabricate integrated 3D constructs. The precise tuning of the rheological properties of these materials is important to make them suitable for realize structures with the 3D printing technology.

A viscoelastic response will be desirable, so that the material can flow through the deposition system and then “set” immediately on the build plate [54].

During this project, a natural hydrogel has been used: the silk fibroin solution.

The Silk Fibroin (SF) solution

Natural hydrogels, such as gelatin and collagen, and synthetic hydrogels, such as poly(ethylene glycol) or PEG, are widely used in bioprinting. In any case, progresses in this field are slowing down due to limited choices of new biomaterials for cell encapsulation and cytocompatible gelation mechanisms.

The silk fibroin solution is a natural hydrogel, derived from Bombyx mori cocoons, that has shown to be high biocompatible (support good cellular attachment and function) which make it extremely attractive as drug and cell carrier, and specifically for the design and fabrication of tissue constructs. Usually hydrogels are especially used for repairing and regenerating soft tissue due to their feeble mechanical properties. In contrast, the silk fibroin solution has a controllable degradability and good mechanical properties; this is proved by the fact that physicians have used silk fibers as a suture material for centuries.

Silk fibroin solution was, therefore, chosen not only for its extraordinary mechanical properties and biocompatibility but also because it represents a new material with proven quality for bioprinting in tissue engineering.

Bombyx mori (silkworm) silk is a unique material composed by two different proteins: the sericin and the fibroin protein. Sericin is a group of soluble glycoproteins expressed in the middle silk gland of Bombyx mori. The fibroin, coated by sericin proteins, instead represents the core of the cocoon silk filament. In literature, sericin has shown to cause immune responses. This is why it must be removed from the fibroin to assure biocompatibility.

Silk fibroin is a block copolymer rich in hydrophobic β-sheet forming blocks linked by small hydrophilic linker segments or spacers. The result is a hydrophobic protein that self-assembles to form strong and resilient materials.

Once the extracted silk fibroin is processed into an aqueous solution, the resulting water-based silk fibroin solution can on one hand be chemically modified to change its surface properties immobilizing growth factors and on the other hand can be properly mixed with other materials to improve its properties and be used in different fields [55]. From the bioprinting point of view, the main challenge of employing the

silk fibroin solution was shaping it in predesigned geometries with a certain layer thickness.

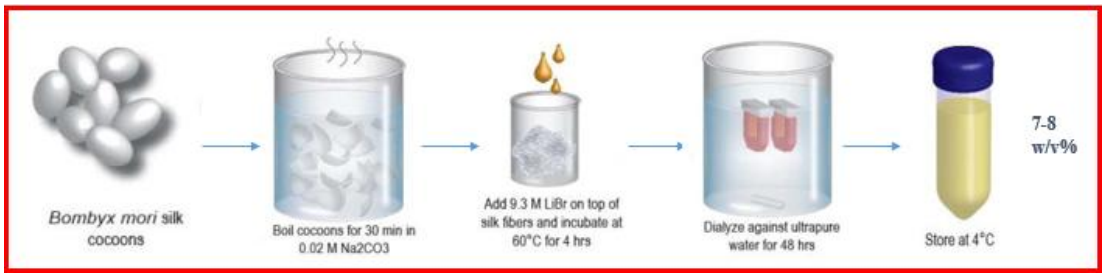

Figure 18 Schematic of the silk fibroin extraction procedure. Starting from the raw material (cocoons) to the final aqueous-based 7-8 w/v% solution will take 4 days [55]

After the removal of the sericin and the extraction of the silk fibroin from B. mori cocoons, a 7-8 w/v% solution is usually obtained, as shown in Fig. 18.

The 7-8 w/v% silk fibroin solution behaves like a Newtonian fluid, disclosing a constant viscosity almost equal to that of the water [56]. It was useful during the modelling of the system but not afterwards.

A particular challenge for the application of silk fibroin solution in extrusion bioprinting was therefore to find a suitable concentration that could meet the previous conditions for accurate printing and also support cell viability and function. Printing fidelity generally increases with polymer concentrations and cross-link density. The silk fibroin solution was, indeed, concentrated up to a 24-26 w/v%. It is possible to find the whole protocols, that to make the silk fibroin solution and that to concentrate it, in the attachment C.

The final step of the whole process is usually to induce crystallinity. There are two main methods to induce crystallinity for the silk fibroin solution: immersion in an alcohol or by water annealing. The used alcohol can be methanol or ethanol; instead, water annealing consists in incubate the structure in a humid environment for several hours. Gelation in this kind of bioink can also be induced via other mechanisms: enzymatic crosslinking by mushroom tyrosinase, a cytocompatible gelation mechanisms or by physical crosslinking via sonication [57].

The silk fibroin solution can be used in different applications, such as: tissue engineering, disease models, implantable devices, and drug release.

In 3D bioprinting, silk fibroin solution has mainly been used in the last few years by mixing it with gelatin. Das S. et al (2014), for example, developed clinically relevant sized tissue analogs by 3-D bioprinting, delivering human nasal inferior turbinate tissue-derived mesenchymal progenitor cells encapsulated in silk fibroin-gelatin (SF-G) bioink [57]. While Chameettachal S. et al. (2016) explored chondrogenic differentiation and suppression of hypertrophic differentiation in tyrosinase cross-linked silk-gelatin bioink using different cell modalities [58].

CHAPTER 5
RESULTS AND DISCUSSION

The system, constituted by the Felix 3.0 dual extruder 3D printer and the Discov3ry universal paste extruder, was characterized in terms of deposition parameters such as material viscosity, line width and height. Numerous limitations have been encountered due to the nature of the system and the choice of material used. Nevertheless the system has shown good potential to be adopted in the field of 3D bioprinting; moreover, it is easy-to-use and not so much expensive. Firstly the results related to the rheological properties of the material are shown; then those regarding the lateral and vertical resolution of the system. The correct ink composition and rheological behaviour have indeed a great impact on the realization of the system for proper extrusion, on its line width and height. All the shown results were compared to those found in literature and properly justified.

Ink Rheology

The optimized system prints hydrogel complex 3D structures layer by layer using a constant-displacement (piston-driven) extrusion mode. A uniform volumetric flow rate is achieved by mechanically applying on the plunger of the syringe the correct pressure to maintain the desired flow conditions. This operational mode is typically of the direct ink writing filament-based techniques that use highly concentrated ink (40-55%) [38].

Highly concentrated ink have shown to be excellent materials for this kind of applications because they have tailoring properties that make them suitable to both freely flow through the nozzle and realize specific patterns that maintain their shape. The viscoelastic response of the material is, indeed, very important and must be carefully controlled.

In fused deposition modelling the fluid-to-solid transition is driven in the print head where the heated polymer liquefies and comes out sitting on a print bed which can be at room temperature, or lower temperature, and essentially solidifies. In DIW filament-based techniques, the material is extruded trough a conical or cylindrical nozzle under pressure at room temperature. In the nozzle the material is exposed to a high shear rate (the highest shear rate is at the nozzle's walls), instead as it is extruded and sit on an underlying printed layer or on the substrate, it goes back to zero stress condition.

The ink flows into the system thanks to a pressure gradient (ΔP) [Pa] and a radially varying shear stress [Pa] is developed [39]:

$$\tau_r = \frac{r\Delta P}{2l}$$

Where r is the radial position within the nozzle [m] (r = 0 at the center axis and r = R at the nozzle wall) and l is the nozzle's length [m].

Consequently, the need to concentrate the solution for filament printing arises from the fact that a shear thinning response of the material is required.

This means that if we increase the pressure or the speed at which we are printing above a certain shear yield stress, the ink will start to flow with an ever-decreasing viscosity and so it will be easier to print, as it is described by the following formula [39]:

$$\tau = \tau_y + K\dot{y}^n$$

Where τ is the shear stress [Pa], τ_y is the shear yield stress [Pa], K is the viscosity [Pa s], ẏ is the shear rate [s^{-1}] and n is the shear thinning exponent (<1).
But interestingly, once the ink exits the nozzle, it goes back to zero shear stress condition and it will be solid-like. So immediately, just by tailoring the viscoelastic properties of the ink, it is possible to print and solidify in one step. The correct tuning of the rheological properties of the material is also important to minimize drying-induced shrinkage of the final structure and maintenance of the shape of the printed line without undesirable spreading of the ink.

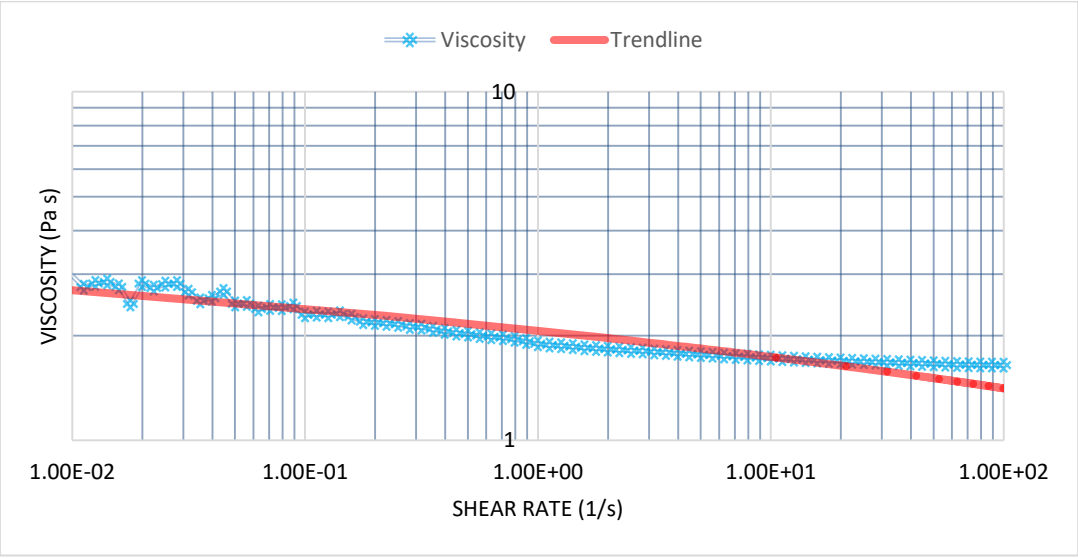

Figure 19 Log-log plot of viscosity as a function of shear rate for the 25 wt% silk fibroin solution

The silk fibroin solution exhibits a very low viscosity at low concentrations (7-8%) behaving more or less like water (around 0.001 Pa s) [56]. It was, therefore, necessary to concentrate the solution to obtain the desired properties mentioned. By

concentrating the solution at 24-26%, it behaves much like a Newtonian fluid with little dependence on the shear rate mostly at low shear rates as shown in Fig. 19. The observed shear thinning behaviour likely reflects the formation of aggregates in solution due to hydrophobic/hydrophilic interactions. Silk fibroin is a block copolymer rich in hydrophobic β-sheet forming blocks linked by small hydrophilic linker segments or spacers. As shear rate increases, these blocks become aligned, decreasing the frictional resistance between layers of the laminar fluid that results in shear thinning. The lower viscosity of the 25% was around 1.64 Pa s (three orders of magnitude greater than that of the 7-8% silk fibroin solution). To further investigate the rheological properties of the silk fibroin solution, the elastic shear modulus, or storage modulus, (G') and viscous shear modulus, or loss modulus, (G'') where determined.

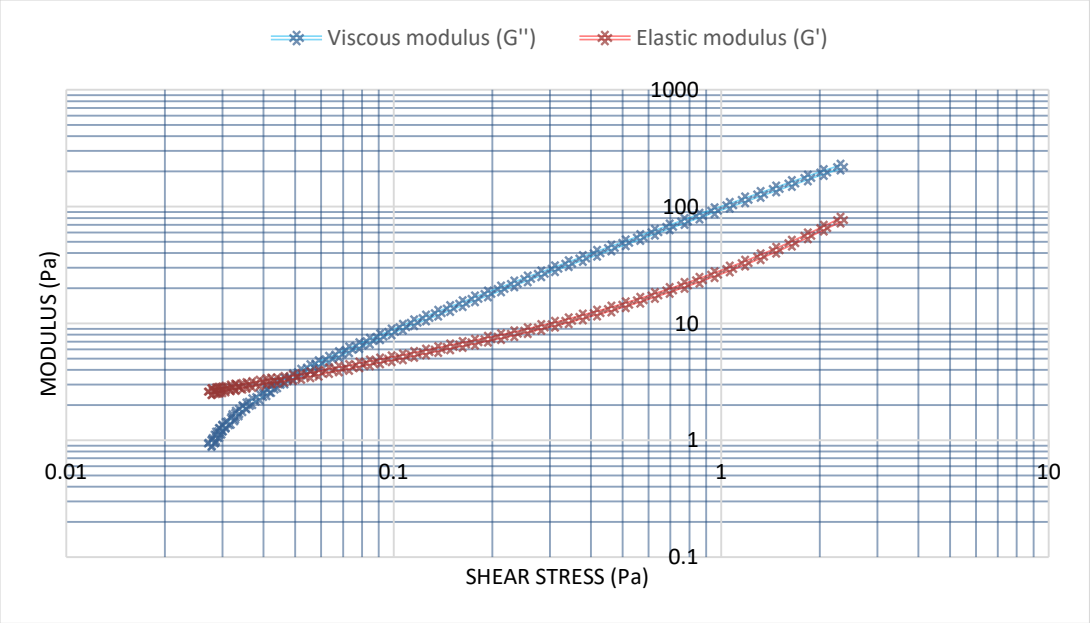

Figure 20 Log-log plot of shear elastic (G') and viscous (G'') moduli as a function of shear rate for 25 wt% silk fibroin ink

As shown from the graph in Fig. 20, the viscous modulus (G'') is higher than the elastic modulus (G') for almost all the shear stresses used in the experimental section. This means that the solution remain liquid-like and it is easy to let it flow through the system. At really low shear stresses, almost zero stress conditions, the

elastic modulus (G') becomes higher that the viscous modulus (G'') and the solution behaves like a gel. The rheological properties of silk fibroin solution were determined using a controlled-stress rheometer (HR-2 Discovery Hybrid Rheometer, TA Instruments) fitted with a 25mm round plate. The viscosity and shear moduli of the 25 % silk fibroin solution were acquired as a function of shear stress (τ) in a logarithmically ascending series of discrete steps. The elastic shear (G') and viscous (G'') moduli of the same silk fibroin ink were measured using an oscillatory logarithmic stress sweep at a frequency of 1 Hz. Measurements were carried out at a temperature of 25 °C with a water solvent trap to reduce drying effects. The shown results are the best achievable with a pure silk fibroin solution but not the optimum ones.

The achieved concentration was 24-26% much lower than that usually used in DIW filament-based techniques. Indeed, the concentration time, for the protocol shown in the attachment C, was not linear, so, in order to avoid the gelling of the silk fibroin solution, it was necessary to do not leave it in the PEG solution for too long. Concentrating the solution further, with a process that resulted at the same time biocompatible and safe for the presented working conditions was not possible. Another approach would be to freeze-dry the solution and treat it with an organic solvent: HFIP (1,1,1,3,3,3-hexafluoro-2-propanol). This method would allow to reach higher concentration simply by varying the proportion of freeze-dried silk and solvent.

HFIP is an highly toxic solvent whose evaporations should not be inhaled. Besides, it has a boiling temperature around 60 °C that, as it will be explained later, it is around the working temperature of the stage. Consequently it was not possible to use this procedure and the 25% silk fibroin solution has been used during this project. It showed good properties for this kind of application but of course not the optimal ones.

Width study

The concentrated silk fibroin solution deposition was achieved through a metallic cylindrical nozzle mounted onto a three-axis, computer-controlled stage. The compound then sits on a stationary heated glass substrate so that the deposited line underwent solidification by induced evaporation of the water content.

As the ink exits the nozzle, the printed lines retain shape even after the evaporation of the water. The viscosity of the concentrated silk fibroin solution was not enough to form a continuous filament that solidifies and maintains the shape immediately after the extrusion of the nozzle as it is expected in DIW filament-based techniques. However, the concentrated solution was flexible enough to maintain a constant flow through the deposition nozzle and adhere to the substrate and underlying layers. In the system, the ink is delivered as discrete droplets of fixed volume that form a continuous line when they come into contact with the glass substrate. The fluid dynamics involved in drop formation and spreading play an important role in the characterization of the system. Drop spreading has a great impact on the thickness of the deposited layer and on the lateral resolution of the printed structures. Droplet spreading is influenced by the porous nature of the underlying build plate or printed structure as well as the time required for a given droplet to solidify after deposition. It can be estimated with the following formula [59]:

$$\frac{r_{max}}{r_0} = \left(\frac{We + 12}{3(1 - \cos\Theta_a) + 4\left(\frac{We}{\sqrt{Re}}\right)} \right)^{\frac{1}{2}}$$

- r_{max} $[m]$: the maximum drop radius after impact;
- r_0 $[m]$: the initial drop radius;
- Θ_a [°]: contact angle between the ink and the substrate;
- We: Weber number (We=$\rho_d v_0^2 d_0/\gamma$);
- Re: Reynolds number (Re=$\rho_d v_0 d_0/\mu_d$).

Where $\rho_d, v_{0,}\, \mu_{d,} d_0$ e γ are the droplet's density [kg m^{-3}], the initial droplet impact velocity [m s^{-1}], the droplet viscosity [Pa s], the characteristic length (i.e., nozzle's diameter) [m] and the droplet surface tension [N m^{-1}] respectively.

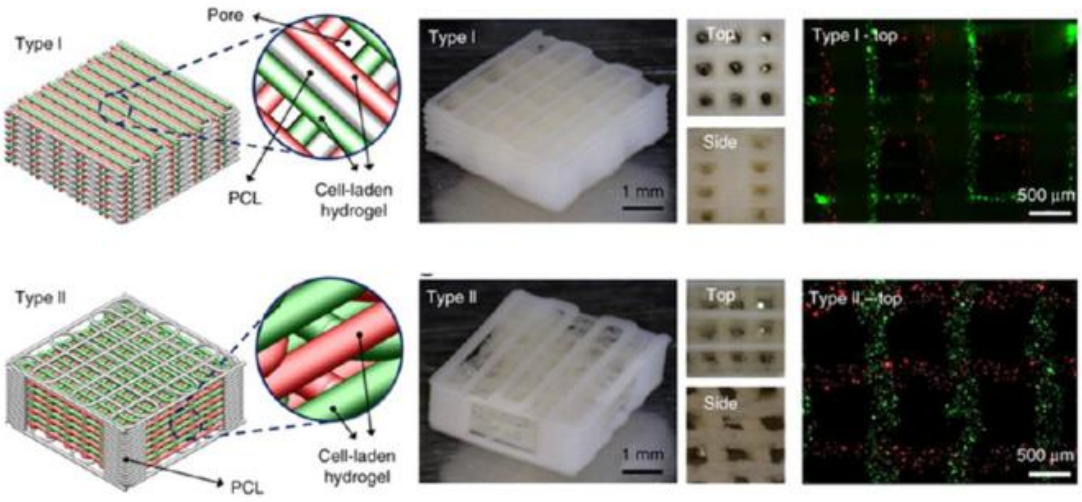

Figure 21 Two types of scaffolds printed with a multimaterial bioprinting system capable of depositing multiple bioinks for fabrication of large-scale vascularized functional tissue constructs [60]

The lateral resolution of the system is determined by the droplet size, the extent of droplet spreading upon deposition on the substrate (or underlying layers), and deformation of the droplet upon solidification. In order to rapidly solidify the droplets, before the spreading occurred, the stage was heated at 40 °C. Nevertheless the droplets underwent negligible solidification before reaching their maximum spread on impact. So to improve print quality, the temperature of the stage was increased from 40°C up to 60-70°C to enhance drying kinetics; however, the dwell times (around 2-3s at 70°C) required from the printed lines to be completely dried were considerable, leading to a significant spreading [61]. Besides, rapid drying of the ink at the nozzle tip led often to clogging. The use of elevated temperatures is, also, not recommended at all when you are working with proteins solution. It would be preferable to reduce the working temperature rather than increase it.

The typical constructs fabricated for bioprintig applications are porous scaffolds with a lateral resolution of the grid structure around 500 µm ([4], [52], [57], [60]), as

shown in Fig. 21. The diameter of the nozzle is usually not smaller than 150–300 μm because a smaller diameter was proved to damage the cells [62].

In order to initially characterize the deposition system, the silk fibroin ink was extruded through a 0.61mm inner diameter (0.9mm outer diameter) nozzle at five different deposition speeds (2 $\frac{mm}{s}$, 2.5 $\frac{mm}{s}$, 5 $\frac{mm}{s}$, 10 $\frac{mm}{s}$, and 15 $\frac{mm}{s}$) onto a stage at 40 °C temperature. Four different flow rates were utilized for each deposition speed (0.1$\frac{mm^3}{s}$, 0.2 $\frac{mm^3}{s}$, 0.3 $\frac{mm^3}{s}$ and 0.4 $\frac{mm^3}{s}$). The gap between the nozzle plate and the printing surface was maintained at 0.1mm by the control program in order to achieve a correct calibration of the stage. The build plate was then moved up of the correct amount, accordingly with the used deposition speed and flow rate. Before to start to print, the silk solution was displaced from the syringe through the print head to the syringe and back several times until no bubbles could be observed in the tubing.

The width of the printed lines was examined by scanning them with an optical microscope and the results are shown in the Tab 2.

Table 2 Average width in μm of 18 lines for each flow rate at a given deposition speed. In the last columns an overall average of the different line widths per each deposition speed and their standard deviation values are reported.

Flow Rate\ Speed	0.1 $\frac{mm^3}{s}$	0.2 $\frac{mm^3}{s}$	0.3 $\frac{mm^3}{s}$	0.4 $\frac{mm^3}{s}$	Average (μm)	Standard Deviation (%)
2 $\frac{mm}{s}$	1083	1013	1000	1066	**1041**	**16.43**
2.5 $\frac{mm}{s}$	924	1030	1021	979	**989**	**16.58**
5 $\frac{mm}{s}$	931	944	914	943	**933**	**17.73**
10 $\frac{mm}{s}$	913	919	967	928	**932**	**16.60**
15 $\frac{mm}{s}$	842	810	888	880	**855**	**15.30**

Changing the flow rate for a given deposition speed, the average line widths were not significantly different between them; so in Tab 2 is reported an overall average of the line widths for each deposition speed. This proves that the slightly difference in the values obtained for the average line widths, at a certain deposition speed changing only the flow rate, is due to a casual error related to the measuring technique used.

Besides of the spreading, another parameter that must be taken into account in the analysis of the width of the printed lines is the shape of the nozzle. It is a cylindrical

metallic needle with an outer diameter (0.91mm) much greater than the inner diameter (0.61mm). The tip of the needle is flat and this can have, together with the spread due to the material's properties, an huge impact on the final width of the lines as a result of the interaction between the tip itself and the material.

A slightly decrease of the line width was noticed instead by varying the deposition speed. Increasing the speed, the line width decrease as shown in Fig 22.

Figure 22 Trend of the line width as a function of the deposition speed

The line diameter is therefore determined by the ink rheology, nozzle diameter and printing speed.

Werner S. et demonstrated that, for a solution of maltodextrin DE5 at 20 and 40wt% in water, greater maximum spread diameters are achieved with the higher impact velocities and lower viscosity droplets [63]. Low viscosity solutions give more extensive spreading as shown in Fig 23.

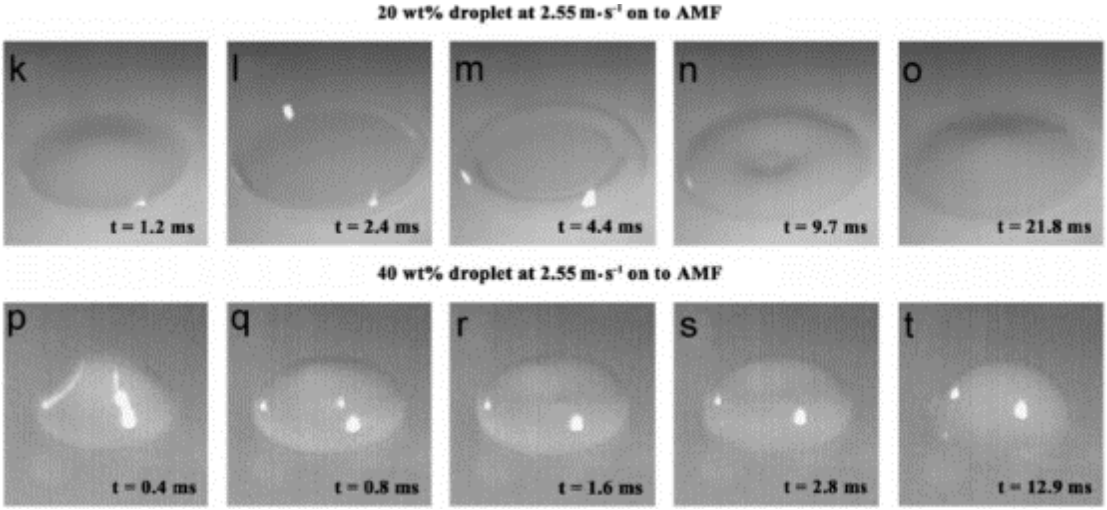

Figure 23 Time series of events depicting the impact, spreading and recoil of various water and maltodextrin DE5 droplet formulations on anhydrous milkfat (AMF) [63].

Consequently, there are two ways to achieve line formation and initial shape retention: tailoring the ink viscosity and drying kinetics.

An initial study for the width of the lines printed with a nozzle of inner diameter 0.266mm (outer diameter 0.5mm) was developed. Few samples at 0.1 $\frac{mm^3}{s}$ flow rate for a deposition speed of 5 $\frac{mm}{s}$ were measured (40 °C stage's temperature). As shown in Fig. 24 the widths of the printed lines is around 500 μm. This is a good resolution for bioprinting applications but a further analysis must be developed for all the flow rate and all the deposition speeds.

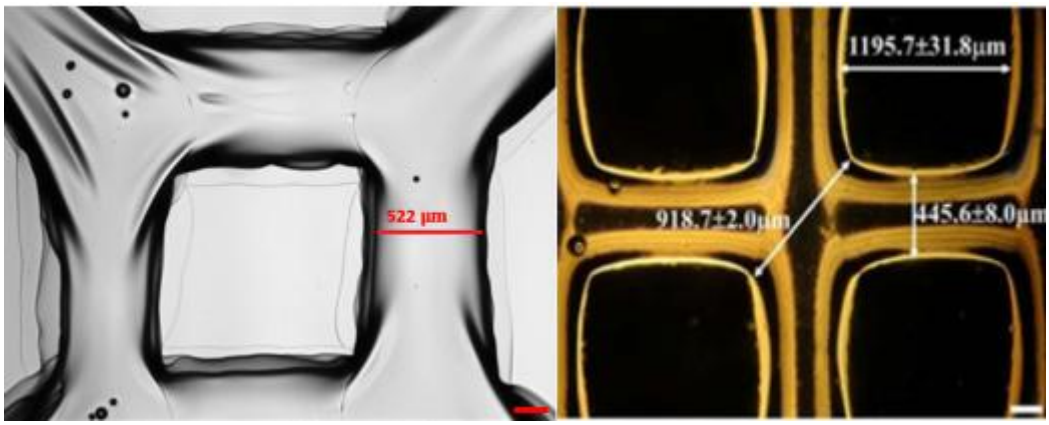

Figure 24 Left: the overall size image of the 3D construct realized with the 25% silk fibroin solution and the nozzle with inner diameter 0.266mm (scale bar 200μm) ; Right: the overall size image of the 3D HCECs /hydrogel construct realized by Wu et al. (scale bar 200μm) [4].

Height study

The vertical resolution (height of the lines) is also determined by the extent of droplet spreading upon deposition on the substrate (or underlying layers) and deformation of the droplet upon solidification. The transition from liquid to the final desired solid material is the final step in the 3D printing process. This transformation is accompanied by a reduction in volume [41]. When solidification occurs by solute evaporation, the volume change may be particularly great if the viscosity of the material is not enough (Fig. 25). Solute distribution during drying can strongly influence the shape of the printed line. The droplet remained liquid during the entire spreading process but the height of droplet's recoil diminishes if the substrate temperature increases [61].

Figure 25 . Starting from the left: Schematics of a theoretical model of dropwise dehydration [64]; Impact of a molten wax droplet with velocity 0.8 m/s on an aluminum surface at temperature 23 °C (centre) and 73 °C (right) [61]

In the graph in Fig. 26 is reported the average height (3 samples per line) for each flow rate (0.1 $\frac{mm^3}{s}$, 0.2 $\frac{mm^3}{s}$, 0.3 $\frac{mm^3}{s}$ and 0.4 $\frac{mm^3}{s}$) at a given deposition speed (2 $\frac{mm}{s}$, 2.5 $\frac{mm}{s}$, 5 $\frac{mm}{s}$, 10 $\frac{mm}{s}$ and 15 $\frac{mm}{s}$) and with a stage's temperature of 40 °C.

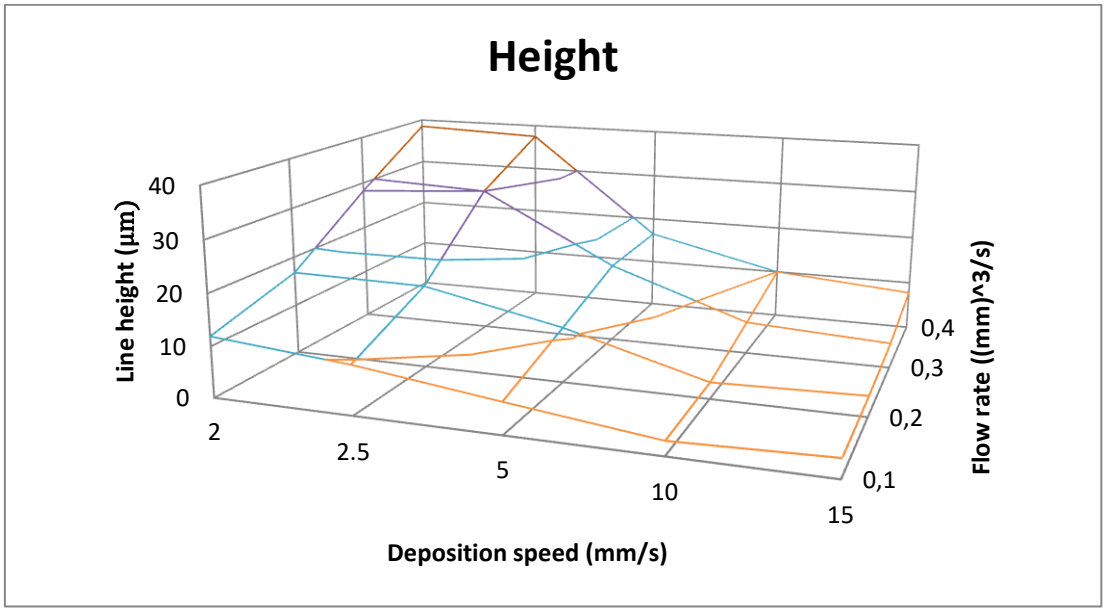

Figure 26 Three-dimensional graph of the line height in function of the different flow rates at each deposition speed.

The lower height is obtained with the lowest flow rate and the highest speed. Increasing the speed for a given flow rate the height of the structure decreases. This is due to the fact that fixing the flow rate, with a certain line width, the height results inversely proportional to the deposition speed [65]:

$$Q = w\ h\ v_0$$

- Q $[\frac{mm^3}{s}]$: flow rate;
- W [mm]: line width;
- h [mm]: line height;
- $v_0[\frac{mm}{s}]$: deposition speed.

When it is deposited the volume of the droplet spreads uniformly in the radial direction from the impingement point. As the droplet achieves the maximum spread to the periphery, the centre begins to rise in height and settles back towards a final end value. This mechanism influences the morphology of the printed lines. The

profile of the lines was examined by an optical surface profiler (Dektak). Thanks to these measurements was also possible to evaluate the height of each line.

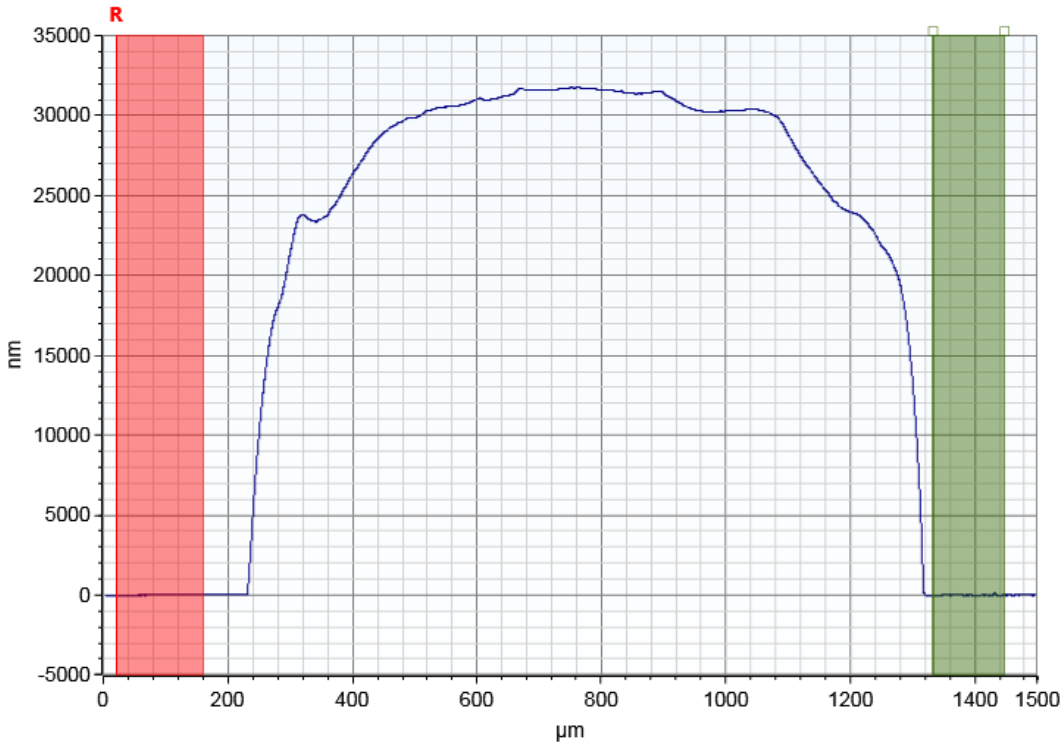

Figure 27 Profile of a 25% silk fibroin line printed at 2 $\frac{mm}{s}$ with a flow rate of 0.4 $\frac{mm^3}{s}$

In Fig. 27 is shown the shape of one of the printed lines. The study of the profile of the lines was really important as a base to start to build layered structures.

Layered structures

After patterning the first layer, the nozzle was incrementally raised in the z-direction to generate the next layer. This process was repeated until the desired 3D structure was formed. 3D periodic structures composed of a simple octogonal geometry were assembled by patterning an array of curved lines in the x-y plane such that their orientation was orthogonal to the previous layer.

The overall structure dimensions were 0.4 – 1.28 mm with 8 – 28 layers as shown in Fig. 28.

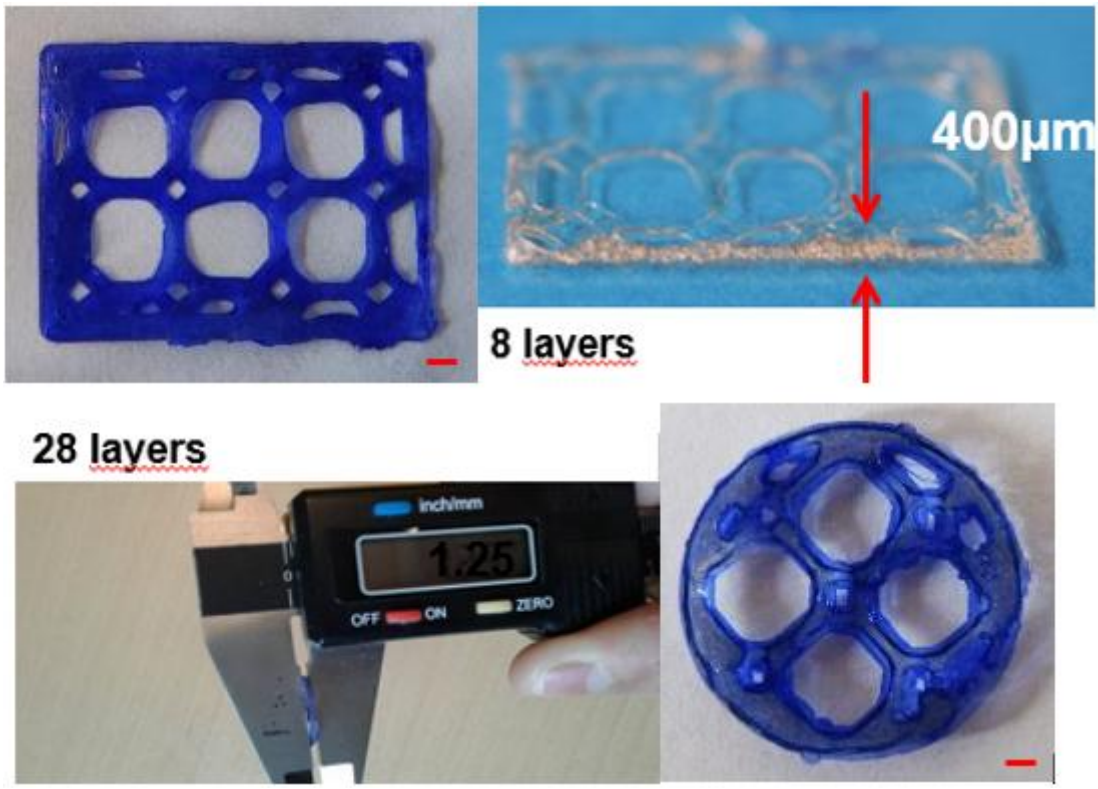

Figure 28 Two different printed structures with different shapes and size. The first with a rectangular shape is 400µm high (8 layers); the second one is circular and is 1.25mm high (28 layers), scale bar, 1mm.

The build time for each structure varied from 30 min to an hour and half, respectively.

The printing rate is limited by the drying or solidification time required for the deposited lines. In order to let them properly dry, it was necessary to stop the print after each layer for at least a minute at 40°C. The interruption of ink flow during assembly is not desirable, so minimize the number of start–stop events is useful.

The software of the printer also controls the plunger motion of syringe pumps holding the ink such that volumetric flow rate is always correct and the system precisely delivers the proper amount of material. Consequently every time that there is the inevitable need to stop the ink flow, the nozzle must be arranged on a new tool path and the flow must be reinitiated before to continue printing in order to achieve again the correct flow rate.

Although the walls of the second structure, for example, had a nominal height of 1.25 mm after printing, the height was not uniform for several reasons.

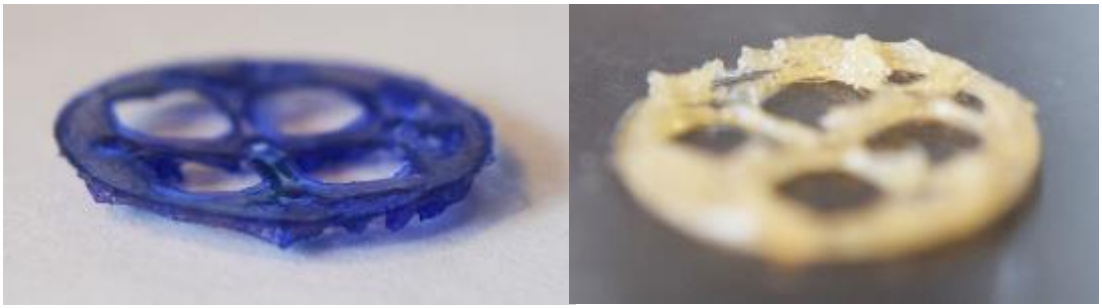

Figure 29 On the left: Profile of a 28-layers silk fibroin printed structure treated with a protein dye containing methanol; on the right: profile of another 28-layers silk fibroin printed structure non treated

Firstly, the ink must "fuse" with the underlying layers. The silk fibroin has shown to be a hydrophobic protein. Consequently when the next layer is deposited, the water-based silk fibroin solution tends to not well attached to the underlying layer forming thinner lines or agglomerates as shown in Fig 29. Secondly the profile of the line is rounded and not perfectly flat. This may allow the material of the next layers to fall down as results of the not optimal support provided.

Figure 30 3-layers silk fibroin printed structure (100μm)

In the 3DP process, removal of the printed structure from the glass substrate is a necessary step that may induce significant dimensional changes in the printed structures. In order to remove faster the structures from the substrate, they were treated with methanol. Methanol is a poor solvent that induces crystallization in the silk fibroin solution. After the methanol treatment the silk fibroin structures started to bend and shrink, becoming easier to crack.

By using a concentrated 24-26% silk fibroin solution as the ink, this effects in the structures were still presented but minimized (Fig. 30) and the overall structures were easier to handle.

CHAPTER 6
CONCLUSIONS AND FUTURE PROSPECTIVES

One important goal for tissue engineering is to produce patient-specific biological tissue substitutes that will repair large or complex tissue defects. Thanks to the presented results, an initial step toward the realization of 3D silk fibroin scaffolds for a numerous array of possible applications has been provided. This might be helpful in the understanding of the role of architectural complexity on tissue development and remodelling. By comparison with other works, the final goal seems to not be so far away.

This work granted important knowledge that can lay the foundations for many future developments.

Firstly, the results show how the rheological properties of the material have an huge impact on the its flow through the system and drying kinetic. A shear thinning response of the material is desirable so that it is possible to print and solidify in only one step.

Secondly, tuning the material concentration or viscosity, it is also possible to modulate the lateral and vertical resolution of the system.

A simple fluid dynamic model has been developed: the line widths and heights depend not only on the given concentration of the material used but also on the applied pressure or extrusion speed and deposition speed, demonstrating the simplicity and the flexibility of this technique.

If the rheological properties of the material are correct, the model, thanks to the perfect flow rate control achieved, enables the prediction of essential topological parameters of the structures deposited (width or height of the printed lines) in function of the amount of extruded material and the deposition speed.

At high viscosities or concentrations, correspond greater height and small widths.

To achieve high resolutions, it is thus necessary to use viscous solutions with low spreading rates. The major limitations in the use of a low viscous solution during the project has been, a part for the spreading, the fact that it tended to drip out of the syringe tip as discrete drops even without the application of pressure and the relatively small height of the printed layers. After drying, the spread droplet may have a height of <1 μm, as it is for DIW droplet-based techniques, that cannot allow the fabrication of a realistic 3D printed solid also after hundreds of printed layers.

The best lateral resolution obtained with the used system (nozzle's inner diameter of 610 μm and outer diameter of 900 μm) was 850 μm with a deposition speed of 15 $\frac{mm}{s}$ and a height in the range of 4 – 8 μm depending on the flow rate. That is why higher speed were not used (at higher deposition speeds correspond lower layers). A thickness of 40 μm was instead achieved with the same nozzle and a flow rate of 0.4 $\frac{mm^3}{s}$ at 2 $\frac{mm}{s}$ deposition speed.

The third important result concerns the impact that the shape of the syringe tip has not only on the lateral resolution of the system but also on the possibility to use any type of material or material blend.

The minimum line width obtainable is limited by the dimensions of the inner diameter and mainly on the shape of the syringe tip.

For a Newtonian fluid the shear stress, that opposes to the movement of the fluid, is directly proportional to the viscosity of the material. Consequently increasing the viscosity, the shear stress increases and also the difficulty to extrude the material. Changing the shape of the needle is possible to reduce the impact of the shear stress on the motion of the fluid, that is why complete cylindrical nozzles are no more used in literature to print with high viscous materials.

The initial study about the lateral resolution of the deposition system with a 266 µm inner diameter cylindrical needle have brought good results in terms of lateral resolution but a more careful study should be undertaken. If for highly viscous materials a cylindrical nozzle may become unusable, for low viscous ones it could instead be the best solution.

A greater shear stress would allow a better deposition, avoiding trickle phenomena.

The importance of this thesis project was therefore to reveal that is the design of the deposition system to adapt to the properties of the chosen material and not vice versa.

After choosing the application, the correct design of the material, to be mixed or concentrated according to the requirements, is the second fundamental step. At this point, only after a careful assessment of its properties, of the laws that control its flow along the system and its deposition mechanisms, it will be possible to adapt the deposition system according to them. The optimized bioprinting process and conditions, including a temperature, feed rate, dispensing speed, and nozzle diameter, have to be developed according to the types of bioink [66]. In any case, a priori knowledge of the profile of deposited structure is necessary; knowing how the profile of the printed line looks like and how the line width varies in function of the flow rate and the deposition speed is fundamental to achieve high quality prints and better layered structures.

The operating system is user friendly and does not require any professional skill. Once the geometry of the scaffold has been chosen and input to the computer and the syringe is filled with a few milliliters of solution, the structure can be fabricated in the space of half an hour or more depending on the number of layers required, the chosen drying kinetic and the deposition speed.

Looking toward the future, there are many opportunities and challenges for direct ink writing of 3D silk fibroin hydrogel via filament-based approach.

Future investigations into the feasibility of this deposition technique for tissue-engineering purposes will be focused on improving new ink designs, better modelling of ink dynamics during deposition, and enhanced control systems to allow

3D patterning with microscale resolution. The advances could bring numerous benefits such as, higher lateral resolutions, avoidance of harsh processing conditions of temperature or toxic organic solvents, and the ability to precisely control complex architectures. Besides, issues related to efficient mixing and control of the silk fibroin solution are still presented.

Tests for trying to mix the silk fibroin solution with graphene at different concentrations of graphene into silk (1%, 5% of SF/graphene) have been carried out. The results have been rather mediocre because the solution and the particulates formed two distinct phases.

Mixing and concentrating the silk fibroin solution with other substances requires a specific procedure because it can easily be spoiled due to the heat and the stirring.

Finally, if 3D direct ink writing approach has to move from prototyping to large-scale production, implementing multiple print heads is needed to allow the simultaneous creation of several patterned structures from a single printing platform. The design of the holder for the tip of the Discov3ry was, indeed, designed not only to make it stable and easy to calibrate but also to allow the possible use of multiple extruders at one time. That is why we tried to reproduce the design of the hot head of the Felix 3.0 dual extruder, changing it only partially.

Together, these advances will enable the use of the deposition system described to produce functional structures for biological applications.

References

[1] B. K. Gu, D. J. Choi, S. J. Park, M. S. Kim, C. M. Kang, and C.-H. Kim, "3-Dimensional Bioprinting for Tissue Engineering Applications.," *Biomater. Res.*, vol. 20, p. 12, 2016.

[2] Z. Quan, A. Wu, M. Keefe, X. Qin, J. Yu, J. Suhr, J. H. Byun, B. S. Kim, and T. W. Chou, "Additive manufacturing of multi-directional preforms for composites: Opportunities and challenges," *Mater. Today*, vol. 18, no. 9, pp. 503–512, 2015.

[3] R. Lanza, R. Langer, and J. P. Vacanti, *Principles of tissue engineering*, Third edit. 2011.

[4] Z. Wu, X. Su, Y. Xu, B. Kong, W. Sun, and S. Mi, "Bioprinting three-dimensional cell-laden tissue constructs with controllable degradation," *Sci. Rep.*, vol. 6, no. April, p. 24474, 2016.

[5] S. A. Wilson and A. Last, "Management of corneal abresions," *Am. Fam. Physician*, vol. 70, no. 1, pp. 123–130, 2004.

[6] A. A. Maximow and W. Bloom, "A textbook of histology," *Am. J. Med. Sci.*, vol. 218, no. 5, p. 598, 1949.

[7] A. Kobayashi, H. Yokogawa, and K. Sugiyama, *Confocal Laser Microscopy - Principles and Applications in Medicine, Biology, and the Food Sciences*. 2013.

[8] J. An, J. E. M. Teoh, R. Suntornnond, and C. K. Chua, "Design and 3D Printing of Scaffolds and Tissues," *Engineering*, vol. 1, no. 2, pp. 261–268, 2015.

[9] 3D printing Blog, "3D Printing Technologies: Stereolithography," 2014. [Online]. Available: https://i.materialise.com/blog/an-intro-to-our-3d-printing-technologies-stereolithography/.

[10] E. Sachs, M. Cima, and J. Cornie, "Three-dimensional printing: rapid tooling and prototypes directly form a CAD model," *CIRP Ann. - Manuf. Technol.*, vol. 39, no. 1, pp. 201–204, 1990.

[11] K. Arcaute, B. K. Mann, and R. B. Wicker, "Stereolithography of three-dimensional bioactive poly(ethylene glycol) constructs with encapsulated cells," *Ann. Biomed. Eng.*, vol. 34, no. 9, pp. 1429–1441, 2006.

[12] I. Madrazo, C. Zamorano, E. Magallón, T. Valenzuela, A. Ibarra, H. Salgado-Ceballos, I. Grijalva, R. E. Franco-Bourland, and G. Guízar-Sahagún, "Stereolithography in spine

pathology: a 2-case report," *Surg. Neurol.*, vol. 72, no. 3, pp. 272–275, 2009.

[13] S. Singare, L. Dichen, L. Bingheng, L. Yanpu, G. Zhenyu, and L. Yaxiong, "Design and fabrication of custom mandible titanium tray based on rapid prototyping," *Med. Eng. Phys.*, vol. 26, no. 8, pp. 671–676, 2004.

[14] J. He, D. Li, B. Lu, Z. Wang, and T. Zhang, "Custom fabrication of a composite hemi-knee joint based on rapid prototyping," *Rapid Prototyp. J.*, vol. 12, no. 4, pp. 198–205, 2006.

[15] G. Staffa, A. Nataloni, C. Compagnone, and F. Servadei, "Custom made cranioplasty prostheses in porous hydroxy-apatite using 3D design techniques: 7 Years experience in 25 patients," *Acta Neurochir. (Wien).*, vol. 149, no. 2, pp. 161–170, 2007.

[16] S. A. Skoog, P. L. Goering, and R. J. Narayan, "Stereolithography in tissue engineering," *J. Mater. Sci. Mater. Med.*, vol. 25, no. 3, pp. 845–856, 2014.

[17] F. P. W. Melchels, J. Feijen, and D. W. Grijpma, "A review on stereolithography and its applications in biomedical engineering," *Biomaterials*, vol. 31, no. 24, pp. 6121–6130, 2010.

[18] F. Scalera, C. Esposito Corcione, F. Montagna, A. Sannino, and A. Maffezzoli, "Development and characterization of UV curable epoxy/hydroxyapatite suspensions for stereolithography applied to bone tissue engineering," *Ceram. Int.*, vol. 40, no. 10, pp. 15455–15462, 2014.

[19] S. Schüller-Ravoo, S. M. Teixeira, J. Feijen, D. W. Grijpma, and A. A. Poot, "Flexible and elastic scaffolds for cartilage tissue engineering prepared by stereolithography using poly(trimethylene carbonate)-based resins," *Macromol. Biosci.*, vol. 13, no. 12, pp. 1711–1719, 2013.

[20] B. Dhariwala, E. Hunt, T. Boland, and D. Ph, "Rapid Prototyping of Tissue-Engineering Constructs , Using," vol. 10, no. 9, pp. 1316–1322, 2004.

[21] D. Dean, E. Mott, X. Luo, M. Busso, M. O. Wang, C. Vorwald, A. Siblani, and J. P. Fisher, "Multiple initiators and dyes for continuous Digital Light Processing (cDLP) additive manufacture of resorbable bone tissue engineering scaffolds," *Virtual Phys. Prototyp.*, vol. 9, no. 1, pp. 3–9, 2014.

[22] R. R. Paulsen and K. S. Pedersen, "Image analysis: 19th scandinavian conference, SCIA 2015 Copenhagen, Denmark, june 15-17, 2015 proceedings," *Lect. Notes Comput. Sci. (including Subser. Lect. Notes Artif. Intell. Lect. Notes Bioinformatics)*, vol. 9127, pp. 302–313, 2015.

[23] Y. Lu, G. Mapili, G. Suhali, S. Chen, and K. Roy, "A digital micro-mirror device-based system for the microfabrication of complex, spatially patterned tissue engineering scaffolds," *J. Biomed. Mater. Res. - Part A*, vol. 77, no. 2, pp. 396–405, 2006.

[24] J. W. Choi, R. Wicker, S. H. Lee, K. H. Choi, C. S. Ha, and I. Chung, "Fabrication of 3D biocompatible/biodegradable micro-scaffolds using dynamic mask projection microstereolithography," *J. Mater. Process. Technol.*, vol. 209, no. 15–16, pp. 5494–5503, 2009.

[25] L.-H. Han, S. Chen, G. Mapili, and K. Roy, "Projection Microfabrication of Three-

Dimensional Scaffolds for Tissue Engineering," *J. Manuf. Sci. Eng.*, vol. 130, no. 2, p. 021005, 2008.

[26] A. Ronca, L. Ambrosio, and D. W. Grijpma, "Preparation of designed poly(d,l-lactide)/nanosized hydroxyapatite composite structures by stereolithography," *Acta Biomater.*, vol. 9, no. 4, pp. 5989–5996, 2013.

[27] M. Meccanica, "Fused Deposition Modelling (FDM)." [Online]. Available: http://www.milanomeccanica.com/fdm.htm.

[28] S. H. Masood and K. Alamara, "Development of Scaffold Building Units and Assembly for Tissue Engineering Using Fused Deposition Modelling," *Adv. Mater. Res.*, vol. 83–86, pp. 269–274, 2009.

[29] M. H. Too, K. F. Leong, C. K. Chua, Z. H. Du, S. F. Yang, C. M. Cheah, and S. L. Ho, "Investigation of 3D Non-Random Porous Structures by Fused Deposition Modelling," pp. 217–223, 2002.

[30] S. G. Alfano, R. M. Taft, and R. F. Robinson, "Fabrication of cranial implants using fused deposition modeling technology," *J. Facial Somat. Prosthetics*, vol. 8, no. 1, pp. 31 – 36, 2002.

[31] E. Kouhi, S. Masood, and Y. Morsi, "Design and fabrication of reconstructive mandibular models using fused deposition modeling," *Assem. Autom.*, vol. 28, no. 3, pp. 246–254, 2008.

[32] X. Ning, Y. Xiaojian, W. Daixu, Z. Jian, C. Yuyun, X. Guohua, and H. Dannong, "3D Artificial Bones for Bone Repair Prepared by Computed Tomography-Guided Fused Deposition Modeling for Bone Repair," *ACS Appl. Mater. Interfaces*, p. pp 14952–14963, 2014.

[33] A. Boschetto and L. Bottini, "Accuracy prediction in fused deposition modeling," *Int. J. Adv. Manuf. Technol.*, vol. 73, no. 5–8, pp. 913–928, 2014.

[34] L. Bochmann, C. Bayley, M. Helu, R. Transchel, K. Wegener, D. Dornfeld, K. J, L. M. and R. D. Bourell D, S. R. and K. J.-P. Levy G, O. R. and M. S. Sood A, H. P. A, R. W. and I. P. Masood S H, K. J. K. S. S. J. and L. S. Ahn D, U. S. and F. R, S. A. J. M. K. A. R. M. and D. D. Clemon L, F. J. C. L. H. N. L. X.-Z. P. S. B. G. K. F. J. N. R. and F. B. Dao Q, E. B. N. R. O. F. S. H. M. E. F. J. N. R. F. B. and J. S. Gregorian A, B. L. H. M. T. R. and D. D. Bayley C, S. L. Website, M. G. M. M. S. Sheet, S. A. H, O. A. and E. Y. M, J. S. and L. E. A. Tong K, L. E. and J. S. Tong K, V. P. and D. J. L. Kruth J, and T. K. K. and H. S, "Understanding error generation in fused deposition modeling," *Surf. Topogr. Metrol. Prop.*, vol. 3, no. 1, p. 014002, 2015.

[35] S. Kalveram, "3D printed silicon carbide for space optics," 2015. [Online]. Available: http://materialsviews.com/3d-printed-silicon-carbide-space-optics/.

[36] D. B. Kolesky, R. L. Truby, A. S. Gladman, T. A. Busbee, K. A. Homan, and J. A. Lewis, "3D bioprinting of vascularized, heterogeneous cell-laden tissue constructs," *Adv. Mater.*, vol.

26, no. 19, pp. 3124–3130, 2014.

[37] Y. Y. Li, L. T. Li, and B. Li, “Direct ink writing of 3-3 piezoelectric composite,” *J. Alloys Compd.*, vol. 620, pp. 125–128, 2015.

[38] J. A. Lewis, “Direct-write assembly of ceramics from colloidal inks,” *Curr. Opin. Solid State Mater. Sci.*, vol. 6, no. 3, pp. 245–250, 2002.

[39] J. A. Lewis, J. E. Smay, J. Stuecker, and J. Cesarano, “Direct ink writing of three-dimensional ceramic structures,” *J. Am. Ceram. Soc.*, vol. 89, no. 12, pp. 3599–3609, 2006.

[40] N. P. Basal and A. R. Boccaccini, *Ceramics and Composites Processing Methods*. 2012.

[41] B. Derby, “Inkjet Printing of Functional and Structural Materials: Fluid Property Requirements, Feature Stability, and Resolution,” *Annu. Rev. Mater. Res.*, vol. 40, no. 1, pp. 395–414, 2010.

[42] S. V Murphy and A. Atala, “3D bioprinting of tissues and organs.,” *Nat. Biotechnol.*, vol. 32, no. 8, pp. 773–785, 2014.

[43] S. M. Peltola, F. P. W. Melchels, D. W. Grijpma, and M. Kellomäki, “A Peltola, S. M., Melchels, F. P. W., Grijpma, D. W., & Kellomäki, M. (2008). A review of rapid prototyping techniques for tissue engineering purposes. Annals of Medicine, 40(4), 268–280. https://doi.org/10.1080/07853890701881788review of rapid prototypin,” *Ann. Med.*, vol. 40, no. 4, pp. 268–280, 2008.

[44] I. Zein, D. W. Hutmacher, K. C. Tan, and S. H. Teoh, “Fused deposition modeling of novel scaffold architectures for tissue engineering applications,” *Biomaterials*, vol. 23, no. 4, pp. 1169–1185, 2002.

[45] Felix printers, “FELIX 3.0 The versatile robust performer.,” 2016. [Online]. Available: http://felixprinters.com/landing/index/view/id/402.

[46] S. P. Animator, “User Manual,” no. September, 2008.

[47] V. D’agostino, *Fondamenti di meccanica applicata alle macchine*, Terza. 2013.

[48] L. G. Griffith and M. A. Swartz, “Capturing complex 3D tissue physiology in vitro.,” *Nat. Rev. Mol. cell Biol.*, vol. 7, no. 3, pp. 211–24, 2006.

[49] V. Mironov, D. Ph, N. Reis, D. Phil, B. Derby, and D. Ph, “Bioprinting : A Beginning,” vol. 12, no. 4, 2006.

[50] M. Nakamura, S. Iwanaga, C. Henmi, K. Arai, and Y. Nishiyama, “Biomatrices and biomaterials for future developments of bioprinting and biofabrication.,” *Biofabrication*, vol. 2, no. 1, p. 014110, 2010.

[51] A. Skardal and A. Atala, “Biomaterials for Integration with 3-D Bioprinting,” *Ann. Biomed. Eng.*, vol. 43, no. 3, pp. 730–746, 2015.

[52] L. E. Bertassoni, J. C. Cardoso, V. Manoharan, A. L. Cristino, N. S. Bhise, W. A. Araujo, P. Zorlutuna, N. E. Vrana, A. M. Ghaemmaghami, M. R. Dokmeci, and A. Khademhosseini, “Direct-write bioprinting of cell-laden methacrylated gelatin hydrogels,” *Biofabrication*, vol.

6, no. 2, p. 024105, 2014.

[53] P. Chi-Chun, B. Arnaud, and P. Yunzhi, “Bioprinting for Tissue Engineering and Regenerative Medicine,” *Mater. Matters*, 2016.

[54] J. A. Lewis, “Direct ink writing of 3D functional materials,” *Adv. Funct. Mater.*, vol. 16, no. 17, pp. 2193–2204, 2006.

[55] D. D. N. Rockwood, R. R. C. Preda, T. Yücel, X. Wang, M. L. Lovett, and D. L. Kaplan, “Materials fabrication from Bombyx mori silk fibroin,” *Nat. Protoc.*, vol. 6, no. 10, pp. 1–43, 2011.

[56] X. Zhang, M. R. Reagan, and D. L. Kaplan, “Electrospun silk biomaterial scaffolds for regenerative medicine,” *Adv. Drug Deliv. Rev.*, vol. 61, no. 12, pp. 988–1006, 2009.

[57] S. Das, F. Pati, Y. J. Choi, G. Rijal, J. H. Shim, S. W. Kim, A. R. Ray, D. W. Cho, and S. Ghosh, “Bioprintable, cell-laden silk fibroin-gelatin hydrogel supporting multilineage differentiation of stem cells for fabrication of three-dimensional tissue constructs,” *Acta Biomater.*, vol. 11, no. 1, pp. 233–246, 2015.

[58] S. Chameettachal, S. Midha, and S. Ghosh, “Regulation of chondrogenesis and hypertrophy in silk fibroin-gelatin based 3D bioprinted constructs,” *ACS Biomater. Sci. Eng.*, p. acsbiomaterials.6b00152, 2016.

[59] K. Seerden, N. Reis, J. Evans, P. Grant, J. Halloran, and B. Derby, “Ink-jet printing of wax-based alumina suspensions,” *J. Am. Ceram. Soc.*, vol. 84, no. 11, pp. 2514–2520, 2001.

[60] Y. S. Zhang, M. Duchamp, R. Oklu, L. W. Ellisen, R. Langer, and A. Khademhosseini, “Bioprinting the Cancer Microenvironment,” *ACS Biomater. Sci. Eng.*, p. acsbiomaterials.6b00246, 2016.

[61] R. Bhola and S. Chandra, “Parameters controlling solidification of molten wax droplets falling on a solid surface,” *J. Mater. Sci.*, vol. 34, no. 19, pp. 4883–4894, 1999.

[62] D. Y. C. Cheung, B. Duan, and J. T. Butcher, *Bioprinting of cardiac tissues*. Elsevier Inc., 2015.

[63] S. R. L. Werner, J. R. Jones, A. H. J. Paterson, R. H. Archer, and D. L. Pearce, “Droplet impact and spreading: Droplet formulation effects,” *Chem. Eng. Sci.*, vol. 62, no. 9, pp. 2336–2345, 2007.

[64] B. Han, G. Y. Yun, J. W. Boley, S. H. Kim, J. Y. Hwang, G. T. C. Chiu, and K. Park, “Dropwise gelation-dehydration kinetics during drop-on-demand printing of hydrogel-based materials,” *Int. J. Heat Mass Transf.*, vol. 97, pp. 15–25, 2016.

[65] G. Vozzi, a Previti, D. De Rossi, and a Ahluwalia, “Microsyringe-based deposition of two-dimensional and three-dimensional polymer scaffolds with a well-defined geometry for application to tissue engineering.,” *Tissue Eng.*, vol. 8, no. 6, pp. 1089–1098, 2002.

[66] F. Pati, J. Jang, J. W. L. Cho, and Dong-Woo, “Extrusion bioprinting,” in *Essentials of 3D Biofabrication and Translation*, 2015.

[67] “Gear ratio.” [Online]. Available: http://arrc.ebscohost.com/ebsco_static/repair-tips/8852CH20_GEAR_RATIOS.htm.

Attachment A

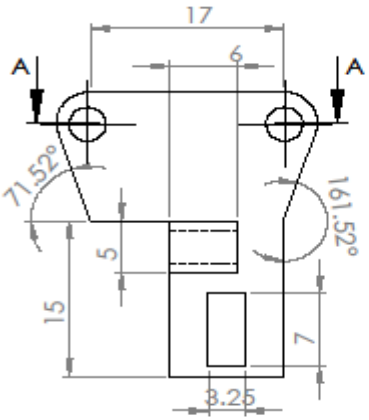

ANTERIOR VIEW

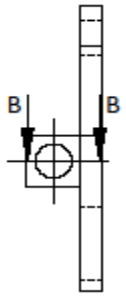

RIGHT VIEW

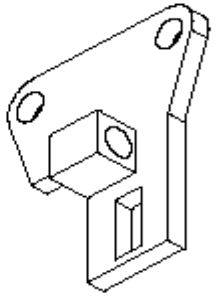

ISOMETRIC VIEW

SEZIONE A-A

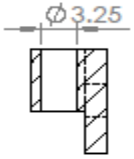

SEZIONE B-B

SOLIDWORKS Educational Product. Solo per uso didattico.

N°	TITLE	
1	HOLDER SUPPORT PART	OPTIMIZATION AND CHARACTERIZATION OF A COMMERCIAL 3D PRINTER FOR DIRECT HYDROGEL WRITING
AUTHOR		
MARIANNA VOLINO		
SUPERVISOR		DESCRIPTION
MARCO CARMINATI		IT IS THE SUPPORT PART OF THE SECOND GENERATION HOLDER
SCALE	ACADEMIC YEAR	
2 : 1	2015 / 2016	

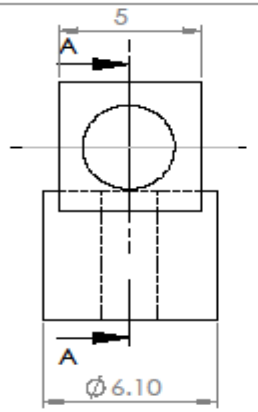

ANTERIOR VIEW

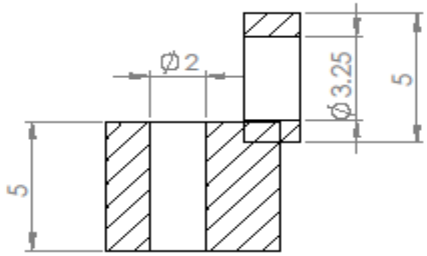

SEZIONE A-A

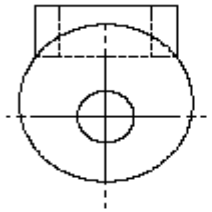

INFERIOR VIEW

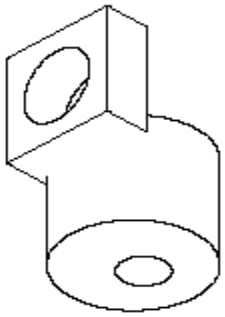

ISOMETRIC VIEW

SOLIDWORKS Educational Product. Solo per uso didattico.

N°	TITLE	
2	HOLDER MOVABLE PART	OPTIMIZATION AND CHARACTERIZATION OF A COMMERCIAL 3D PRINTER FOR DIRECT HYDROGEL WRITING
AUTHOR		
MARIANNA VOLINO		
SUPERVISOR		DESCRIPTION
MARCO CARMINATI		IT IS THE MOVABLE PART OF THE SECOND GENERATION HOLDER
SCALE	ACADEMIC YEAR	
5 : 1	2015 / 2016	

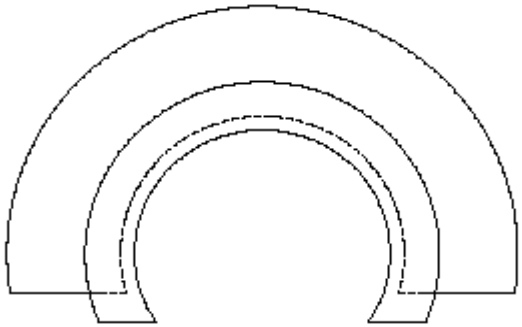

ANTERIOR VIEW

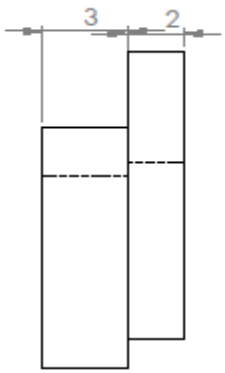

RIGHT VIEW

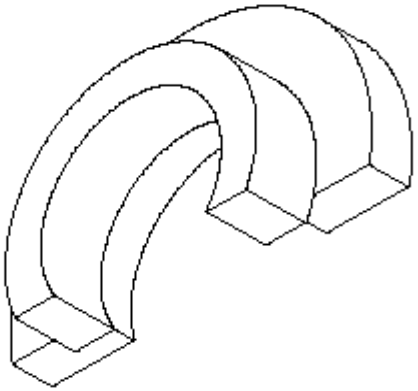

ISOMETRIC VIEW

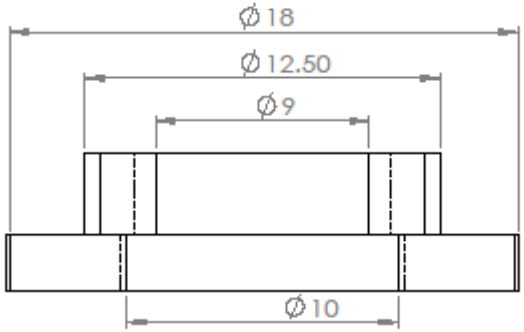

INFERIOR VIEW

N°	TITLE	
3	LOWER-PART-1ml	OPTIMIZATION AND CHARACTERIZATION OF A COMMERCIAL 3D PRINTER FOR DIRECT HYDROGEL WRITING
AUTHOR		
MARIANNA VOLINO		
SUPERVISOR		DESCRIPTION
MARCO CARMINATI		IT IS NECESSARY TO ADAPT THE BASE OF THE DISCOV3RY TO THE PISTON OF THE 1ml -SYRINGE
SCALE	ACADEMIC YEAR	
5 : 1	2015 / 2016	

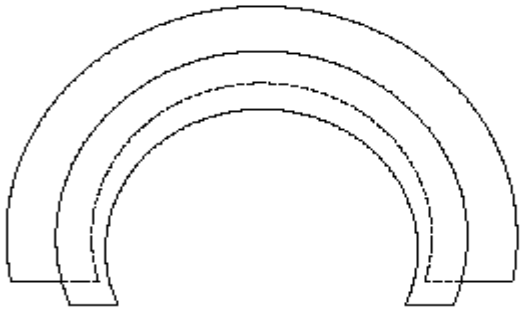

ANTERIOR VIEW

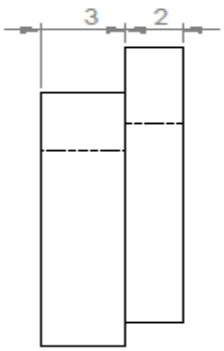

RIGHT VIEW

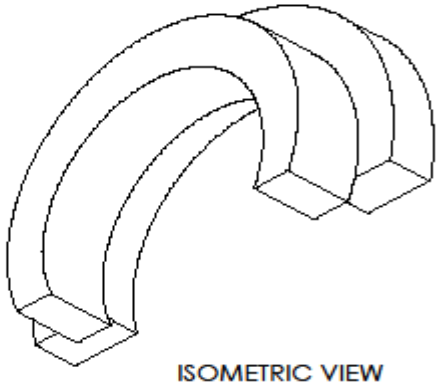

ISOMETRIC VIEW

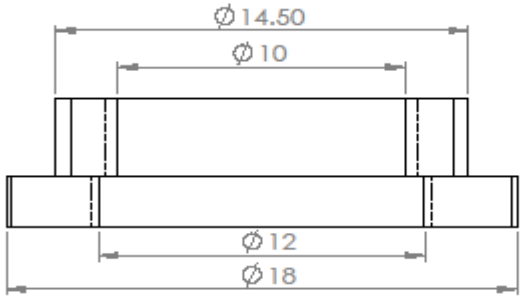

INFERIOR VIEW

N°	TITLE	
4	LOWER-PART-5ml	OPTIMIZATION AND CHARACTERIZATION OF A COMMERCIAL 3D PRINTER FOR DIRECT HYDROGEL WRITING
AUTHOR		
MARIANNA VOLINO		
SUPERVISOR		DESCRIPTION
MARCO CARMINATI		IT IS TO ADAPT THE BASE OF THE DISCOV3RY TO THE PISTON OF THE 5ml SYRINGE
SCALE	ACADEMIC YEAR	
5 : 1	2015 / 2016	

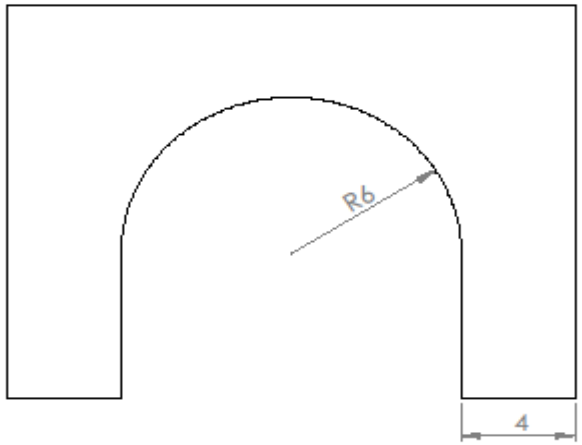

ANTERIOR VIEW

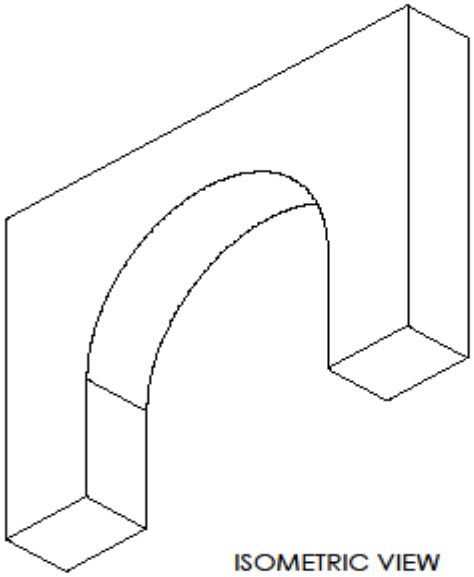

ISOMETRIC VIEW

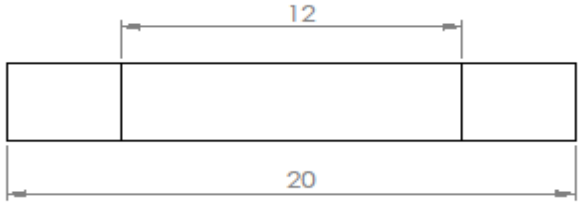

INFERIOR VIEW

N° 5	TITLE: UPPER-PART-5ml	OPTIMIZATION AND CHARACTERIZATION OF A COMMERCIAL 3D PRINTER FOR DIRECT HYDROGEL WRITING
AUTHOR: MARIANNA VOLINO		
SUPERVISOR: MARCO CARMINATI		DESCRIPTION: IT IS NECESSARY TO BLOCK THE 5ml SYRINGE TO THE DISCOV3RY
SCALE: 5 : 1	ACADEMIC YEAR: 2015 / 2016	

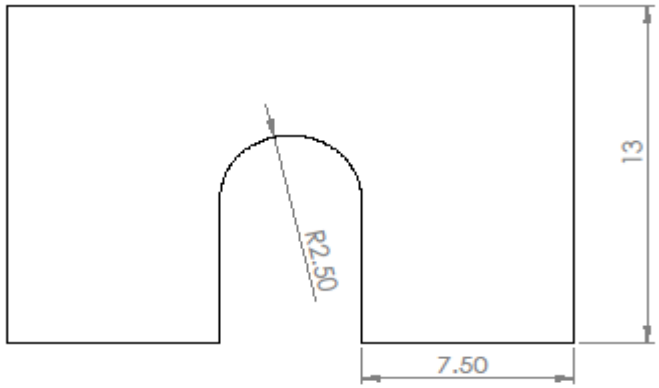

ANTERIOR VIEW

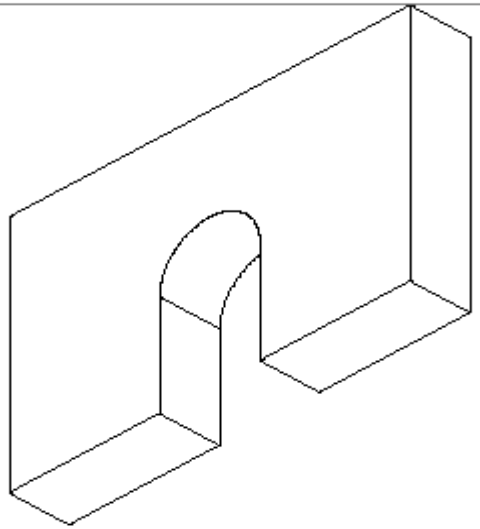

ISOMETRIC VIEW

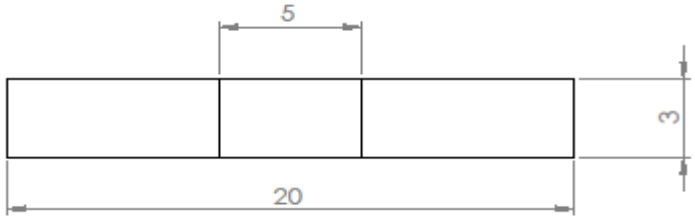

INFERIOR VIEW

N° 6	TITLE: UPPER-PART-1ml	OPTIMIZATION AND CHARACTERIZATION OF A COMMERCIAL 3D PRINTER FOR DIRECT HYDROGEL WRITING
AUTHOR: MARIANNA VOLINO		
SUPERVISOR: MARCO CARMINATI		DESCRIPTION: IT IS NECESSARY TO BLOCK THE 1ml SYRINGE TO THE DISCOV3RY
SCALE: 5 : 1	ACADEMIC YEAR: 2015 / 2016	

Attachment B

Printer software: Repetier-Host

Repetier-Host is a program that provides the following functions:

- Control of the 3D printer, move axis and set temperatures, monitoring etc.
- Process CAD files (STL files) and make them printable.

There are essentially four main tabs in Repetier-Host: object placement, slicer, g-code editor and manual control. Object placement allows to add the stl file, scale the object, rotate and move it along the build plate etc. In the slicer tab is possible to slice the structure; that means chop up the solid stl file into layers and set all the different parameters that characterize each layers (height and width of the layer, speed of the printer, printing temperature etc.). The slicing procedure creates the G-code which is what the printer runs off. In the G-code editor tab is then possible to read and modify the whole G-code. Manual control tab shows the printer progress. In this tab there are also buttons that move around the printer, home buttons that zero the position of the hot-end along each axis, feedrate and flowrate scroll bars that adjust respectively the printer's speed and the extrusion's speed during the print and others kind of buttons and scroll bars, such as those to control the temperature both of the bed and of the hot-ends.

The slicer: KISSlicer

Among the operations that Repetier-Host allows to perform, the slicing is certainly the most important one. You can choose according to the preferences, which slicer use among those suggested from the program (Slic3r, CuraEngine) or any other external slicer.
During this thesis project, KISSlicer has been used.
KISSlicer is a fast and easy-to-use program that takes 3D files (Stl) and generates path information (G-code) for a 3D Printer. The free version has all the features needed for the use of a single-extruder machine; the PRO version, that is not free, instead adds multi-extruder printing. The main settings for this thesis project are described below [47]:

- Style:
  - Extrusion width [mm]: is the opening size of the nozzle (the nozzle diameter);
  - Infill Extrusion width [mm]: is the desired width of the printed line. It should always be greater than the nozzle diameter. Wide extrusions speed up the prints, but do not allow a good level of detail. On the other hand, thin extrusions allow a good detail but can make fragile part and require lower speeds;
  - Layer Thickness [mm]: is the desired height of the layer. At the beginning of each layer the build plate moves down of this amount.
- Material:
  - Diameter [mm]: is the diameter of the filament that is load inside the printer;
  - Main temperature [°C]: hot-end's temperature for the entire print;
  - First Layer temperature [°C]: hot-end's temperature for the first layer only;
  - Bed temperature [°C]: the temperature of the build plate;

- **Flow Tweak**: it may happen that in spite of the precise measurements of the diameter of the filament, the results are still unsatisfactory (prints "fat" or "thin"). With this parameter, you can compensate for this behaviour. The default value is 1, you can slightly increase it (ex:1.05) if you see space between the extrusion lines or decrease it if the nozzle is sailing between molten polymer waves.
- Prime [mm]: the amount of filament to be extruded before starting the actual printing of each layer. The value must be equal to or greater than the next parameter.
- Suck [mm]: the amount of filament to be unplug at the of the printing of each layer.
- Wipe [mm]: the length of the backward path to clean the nozzle at the end of the printing.

- Printer:
  - Z-offset [mm]: if you want to print higher or lower in reference to where the bed is, you can change this parameter and add an offset;
  - Speed [$\frac{\text{mm}}{\text{s}}$]: it is possible to set the speed's values of the printer head and of the build plate for the perimeter and the infill of each layer.
- Gcode: in this section of the program is possible to personalize and modify the whole generated G-code.

The G-code

The G-code, or G programming language, is a numerical control (NC) programming language. It is used mainly in computer-aided manufacturing to control automated machine tools, like a 3D printer.

The G-code is the language that defines the instructions on where to move, how fast to move, and what path to move both the 3D printer head and the build plate.

A typical piece of Gcode might look like this:

```
G1 X50 Y25.3 Z13.8 E22.4 F3000
```

Where:

- G1: means linear movement;
- X50: indicates the position in mm to move to on the X-axis;
- Y25.3: indicates the position in mm to move to on the Y-axis;
- Z13.8: indicates the position in mm to move to on the Z-axis;
- E22.4: the amount of material in mm to extrude between the starting point and the ending point;
- F3000: the feedrate (printer head's and build plate's speed) in mm/min between the starting point and the ending point.

The Gcode is, therefore, a list of fields (G X Y Z E F ..) that are separated by white spaces. A field can be interpreted as a command, a parameter, or for any other special purpose. It consists of one letter directly followed by a number, or can be only a stand-alone letter (Flag). The letter gives information about the meaning of the field. Numbers can be integers (128) or fractional (12.42), depending on context. For example, an X coordinate can take integers (X175) or fractionals (X17.62), but selecting extruder number 2.76 would make no sense.

Attachment C

Protocol: how to make the SF solution

The protocol "Materials Fabrication from Bombyx mori Silk Fibroin" describes the method to first remove the sericin and extract silk fibroin from B. mori cocoons in order to fabricate hydrogels for scaffolding in tissue engineering. The fibroin fibers, indeed, are dissolved into an aqueous solution that can be further processed into different materials. The extraction process takes 4 days [58]:

1) Prepare a 2 L glass beaker filled with 2 L of ultrapure water, cover with aluminum foil, and heat until boiling.
2) Cut the cocoons and measure out 5g of cocoon pieces into a large weigh boat.
3) Add 4.24g of sodium carbonate to the water and let it completely dissolve (to make a 0.02 M solution of Na_2CO_3).
4) Add the cocoon pieces once the water starts to boil and cook it for 30 minutes. Occasionally, stir it with a spatula to promote good dispersion of fibroin.
5) Remove the silk fibroin with a spatula and cool by rinsing in ultrapure water. Squeeze excess water out of the silk. Discard the sodium carbonate solution in the sink.

6) Put fibroin in a 1 L beaker filled with 1 L of ultrapure water and a stir bar. Rinse the fibroin in water for 20 minutes while gently stirring on a stir plate. Repeat this twice for a total of 3 rinses.
7) After the third wash, remove the silk, squeeze it well, and then spread it out on a clean piece of aluminum foil.
8) Allow the silk fibroin to dry in a fume hood overnight.
9) Prepare a 9.3 M LiBr solution.
10) Let fibroin dissolve in an oven at 60°C for 4 hours.
11) Insert 12 mL of the silk-LiBr solution into a 3-12 ml dialysis cassette. Dialyze against 1L of ultrapure water per 12 ml cassette. To ensure mixing, use a large stir bar and place on a magnetic stir plate. Change water after 1 hr, 4 hrs, that evening, the next morning and night, and in the morning on the following day (6 changes within 48 hours).
12) Remove and place silk in a 50 ml conical tube.
13) Centrifuge to remove impurities. Place in a centrifuge and spin at 9,000 rpm (approximately 12,700 g) at 4°C for 20 minutes.
14) Carefully remove tubes from the centrifuge and either pour or transfer the silk solution into another centrifuge tube. Be sure to leave any white flocculent or brown matter behind.
15) Repeat steps 13-14 again.
16) In order to determine the concentration of the silk in solution, measure the weight of a small weigh boat. Then add 0.5 ml of the silk solution to the boat and allow it to dry at 60 °C. Once the silk is dry, determine the weight of the silk and divide it by 0.5 ml. This will yield the weight per volume percentage. A batch of 5 g of silk cocoons generally yields 25 ml of **7-8 w/v% silk solution**.

The silk solution can be stored at 4°C for at least a month. The protocol is described for one batch of 5 grams of silk cocoons but if more material is required, the volumes can be scaled appropriately. The properties of the solution can vary depending on the length of the boiling time and the source of the silk.

Protocol: how to concentrate the SF solution

The silk fibroin aqueous solutions can also be concentrated within an additional 14 hours [68]. The silk fibroin solution (8wt%) is dialyzed against a 15wt% poly(ethylene glycol) (PEG) (8000 g mo1, Sigma Aldrich) solution at room temperature by using Slide-a-Lyzer dialysis cassettes (MWCO 3500).

The volume ratio of PEG solution to silk fibroin solution is 40:1.

After approximately 14 h, the concentrated silk fibroin solution is slowly removed by a syringe to avoid excessive shearing.

All solutions can be stored at 4 °C.

The amount of time used to concentrate the solution may need to be altered for each batch. The concentration time is not linear, so care must be taken to avoid gelling the silk in the cassette if left in the PEG solution for too long [58].

ACKNOWLEDGEMENTS

First of all, I would like to thank Professor Marco Carminati who allowed me to undertake this experience and, with his lectures, convinced me to pursue electronic studies. Thanks for the all help provided, and the concrete support to the objectives set out in this thesis work and for the great moral support.

I would also like to thank Professor Jenny Emnéus for the valuable advices, for the great trust and freedom she gave me in the development of this thesis project and for have always considered my opinion, making me work in a peaceful and inspiring environment.
Thank you, I will never forget our trip to Holland.

A great thanks also goes to Professor Arto Heiskanen who has patiently followed the development of the thesis and provided me with valuable suggestions, supporting me in the difficult times.

I would like also to thank Ada and Vida for all the nice conversations and all the candies that you have given me. They helped me a lot.
A special thanks goes to Ada for her invaluable help in making the latest measurements. Thank you.